An Active Feedback Target Engagement System for Laser-IFE

Lane C. Carlson

9 March 2006

UNIVERSITY OF CALIFORNIA, SAN DIEGO

An Active Feedback Target

Engagement System for Laser-IFE

A thesis submitted in partial satisfaction of the

requirements for the degree Master of Science in

Engineering Sciences (Mechanical Engineering)

by

Lane C. Carlson

Committee in charge:

    Professor Mark S. Tillack, Chair
    Professor Farhat Beg
    Professor George R. Tynan

2006

The thesis of Lane C. Carlson is approved:

_____

_____

_____
                                                         Chair

University of California, San Diego

2006

TABLE OF CONTENTS

LIST OF FIGURES

LIST OF FIGURES

ABSTRACT OF THE THESIS

An Active Feedback Target

Engagement System for Laser-IFE

by

Lane C. Carlson

Master of Science in Engineering Sciences (Mechanical Engineering)

University of California, San Diego, 2006

Professor Mark S. Tillack, Chair

Uniform and symmetric illumination of an inertial confinement fusion (ICF) target by many independent laser driver beams is essential for direct-drive ignition. This requires all beams to converge and focus on the target, which is traveling at more than 50 m/s, with both high precision and accuracy in space, each within a given error envelope of $\pm$ 20 μm rms for all beams. This, in turn, dictates a system that will be able to track the target in three dimensions and a beam steering system to steer and align the lasers so they converge on a single point in space that will be occupied by the target at chamber center. This work focuses on building and characterizing such an active feedback beam steering system and demonstrating feasibility with a tabletop demonstration.

The basis of tracking the target is to illuminate it with a collimated laser beam and detect the presence of a diffraction phenomenon known as the Poisson spot on a CMOS (complementary metal oxide semiconductor) camera. The Poisson spot is an intense diffraction pattern that occurs when a sphere is illuminated by a collimated Gaussian beam. In the far field, the intense spot of light is exactly on axis with the sphere and exists at all points along the line of light. We have been able to track the centroid of the Poisson spot, and thus the target, to better than $\pm$ 5 μm with an update rate of 30 ms.

The next step is to use a simulated driver beam representing the proposed driver for the laser-IFE power plant to engage the target. The centroid information gained from the Poisson spot tracking system is used to steer a fast steering mirror to illuminate the target as it comes into the chamber center, thus simulating a pulse from the laser. To replicate the target in motion, we have built a slow-speed target transport device that moves the target along a rail. We have successfully demonstrated continuous, on-axis target tracking and steering with an update rate of 40 Hz.

Recommendations for improving speed and accuracy for the next generation of hardware and software are given, as well as a more prototypic way to move the target. We have concluded that the proposed engagement concept is viable by demonstrating proof-of-principle experiments. We have reasonable expectations that this engagement concept will work in an IFE power plant.

I. Introduction

I.1 Laser ICF Overview

The underlying principle for inertial confinement fusion is to inject targets filled with deuterium and tritium at cryogenic temperatures into a reaction chamber where the target is heated with a uniform array of high-energy lasers. The lasers cause an ablation inward of the surface, thus imploding and compressing the target thousands of times its nominal density and temperature. At the center of these conditions, a thermonuclear reaction occurs and a burn front propagates outward while consuming the D-T fuel. The released energy in the form of neutrons, charged particles, and electromagnetic radiation is captured by the chamber wall and converted into electrical energy through a turbine-generator configuration. Figure 1 below shows a block diagram of such an IFE power plant.
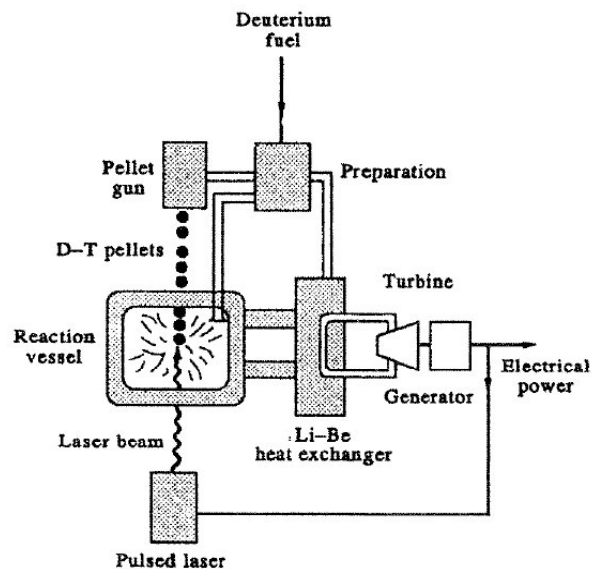
Figure 1 - Laser-IFE power plant block diagram [1]

Uniform and symmetric illumination by the multiple laser driver beams of an ICF target is essential for direct-drive ignition. If the beams do not heat the target uniformly, then the compression will be unbalanced and the necessary thermonuclear conditions will not be met. This leads to a necessary requirement for all driver beams to converge and focus on the target precisely in space and time, each within a given error envelope, to ensure complete and uniform illumination (see figure 2 below). This in turn necessitates a highly precise and highly accuracy target engagement system that is able to continuously track the target in-flight as well as steer the driver beams to converge uniformly on the target when it comes into chamber center.
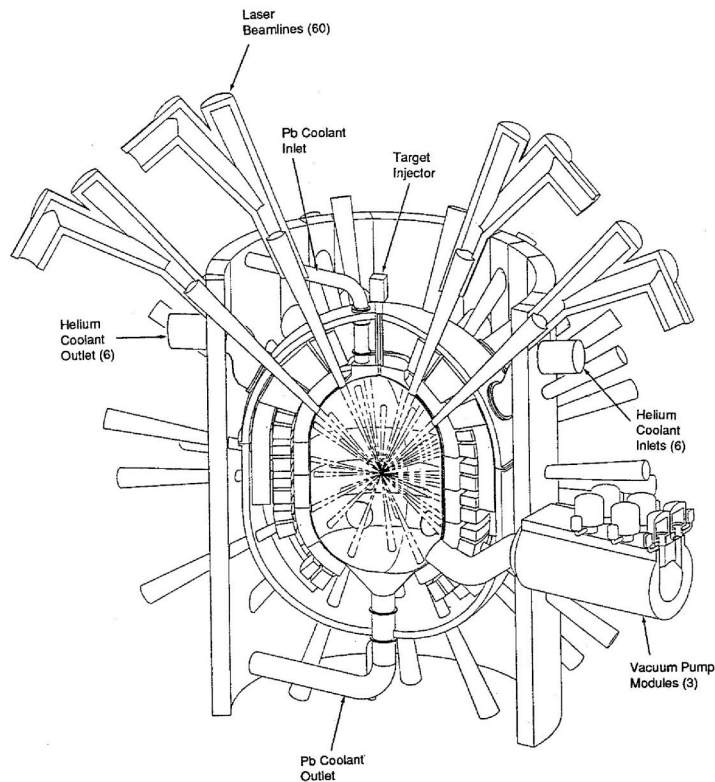
Figure 2 - Prometheus-L reactor showing multiple laser beamlines converging at chamber center [2]

This work focuses on the characterization and demonstration of such a target tracking and active feedback beam steering system. This system has been designed in part by Graham Flint [3] and is a component of an overall target tracking and engagement R&D plan, to be described below. The demonstration of this engagement system uses a video camera to detect an optical phenomenon called the Poisson spot of the target. The centroid of this spot is calculated by vision software and is used to actuate a fast steering mirror that steers a simulated driver beam onto the moving target. The specific details of each component and subsystem are described below. Recommendations for improvements to the system and future generations of hardware and software are also given.

I.2 Requirement for a Target Tracking & Engagement System

Direct-drive, inertial confinement fusion requires that all laser driver beams converge and focus to within $\pm$ 10 μm on a 4mm target that is traveling more than 50 m/s [4]. Proper and uniform illumination of the target is crucial for successful inertial confinement fusion to take place. Therefore, the position of the target must be known to this high degree of accuracy in space 1-2 ms before the driver lasers fire. The driver beams must all be directed so that they converge on a single point in space that the target is expected to occupy at some future time. There is no feedback from an external reference system or the target except 1-2 ms before it reaches chamber center. At this time, a "glint" laser fires at the target, which provides an instantaneous reference for the final alignment of the diver beams.

The proposed tracking system follows the target continuously at it travels down the injector, updating its position every 10-20 centimeters rather than discretely at a few points along the way. This provides a continuous and accurate prediction of the final position of the target at chamber center, thus allowing the mirrors more time to steer their driver beams precisely to the anticipated target location.

I.3 Prior Tracking Work

Previous to this effort, a first generation tracking system was built using three detectors that measured the target's vertical location perpendicular to its travel, as shown in figure 3 below. The ex-chamber tracking system measured the initial trajectory and velocity of the target with the first two detectors and then predicted, on the fly, the exact position the target was expected to be in at chamber center. A third detector confirmed the predicted and actual locations. This system was able to predict target position to 0.49 mm (1σ) [5].
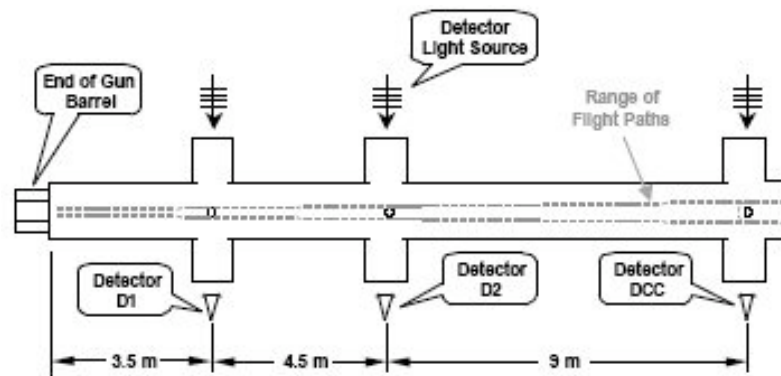
Figure 3 - Ex-chamber tracking system [6]

At that time, it was anticipated that an in-chamber tracking system would be required in the future [6]. It was deemed much more desirable to track the target in-chamber with a continuous update of position and velocity instead of a few discrete tracking points. The ideal tracking system was proposed to be "one in which the target position is defined in terms of displacement from, and location along, a line which joins a pair of fixed points that lie on diametrically opposite sides of the chamber [7]." The basic principle was derived from beam riding techniques that are used to guide military ordinance. This vision has led to the design and development of the Poisson spot and Doppler fringe counting techniques, which are the basis of this next generation target engagement system.

II. Inclusive R&D Plan

II.1 Purpose of R&D Plan

The purpose of the target engagement system is to track the target in three dimensions and steer multiple beamlets to illuminate the target within a certain error budget and time scale. However, the complexity of building such a system begins to become apparent once the details and equipment needed are compounded. It is helpful to break this proposal up into smaller, more manageable subsystems that can be worked on and demonstrated individually, yet combine into the comprehensive engagement plan. The R&D plan is a useful roadmap and learning process for completing the target tracking and beam steering system as a whole.

We have used Flint's engagement design concept from a presentation [3] and paper [7] to devise an R&D plan that lays out the entire proposed target tracking and steering project and defines its fundamental building blocks and critical components. By assimilating such a flow chart or roadmap, as shown in figure 4, it allows for an overall view of the plan and a progressive assimilation of components resulting in a target engagement system with increasing capability.
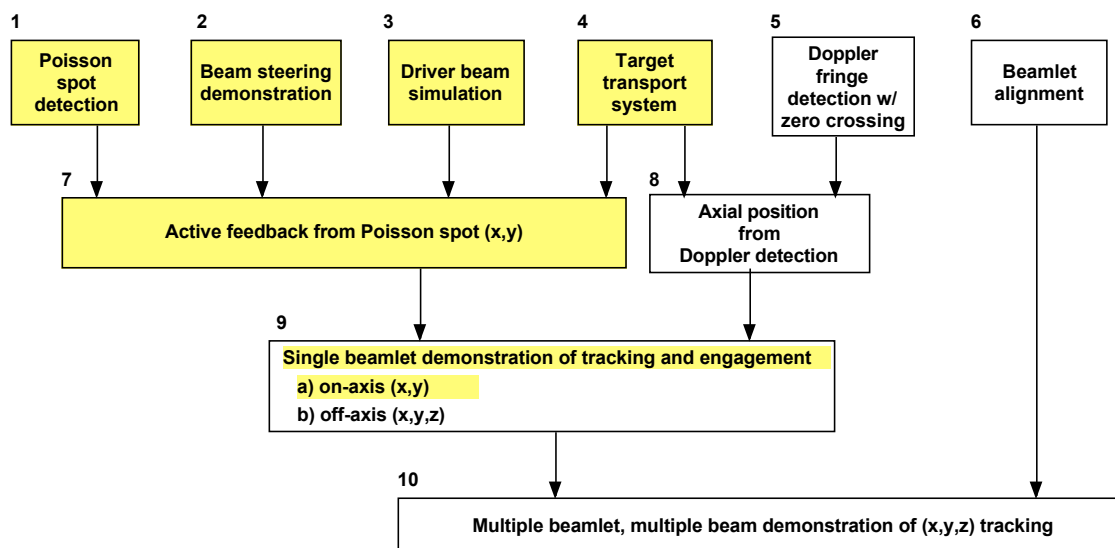
Figure 4 - Target Engagement R&D Plan

II.2 Thesis Components

The goal of this thesis project is to build, characterize, and demonstrate an active target tracking and beam steering system for laser inertial fusion energy (IFE). We propose to build and demonstrate feasibility with a bench-top prototype of a target engagement system using the above-described integrated approach after developing each subtask individually. We have examined one portion of this system to demonstrate its feasibility using active feedback and beam steering from Poisson spot position measurements. The work of this thesis incorporates elements 1, 2, 3, 4, 7, and 9a, as highlighted in yellow. Although all elements of this roadmap need to be completed for a thorough demonstration of a target engagement system, this thesis only encompasses these specific elements, yet consideration and attention is paid toward future incorporation with the other components.

II.3 Requirements & Goals

The defined requirements of this project reflect as much as possible a prototypical system with prototypical speeds, lengths, precision, optical trains, and hardware; however, more stringent requirements come with increasing cost. Therefore, in areas where the requirements cannot be quite met with relatively cheap, off-the-shelf technology, we have rationalized that faster acquisition, computation speeds, and steering can be accomplished if more capital is willing to be spent. Consequently, we have decided to first begin with a low-speed, relatively inexpensive demo to work out details, learn from limitations of our components, and prove that the general target engagement concept works. Then, after recommendations have been made from what we have learned, invest the capital into faster, more capable components that are able to meet the final requirements.

Preliminary target engagement requirements have been established as displayed in table 1 below. The target tracking precision refers to how precise the tracking algorithm must know the location of the target in three-dimensional space. The tracking update rate is the time between target location reports. The steering precision of the driver beamlets is how much rms error is acceptable for pointing all the fast steering mirrors at the chamber center. The final steering time is 1-2 ms after the glint laser fires, right before the lasers fire. Through whatever means used to inject the target, the accuracy is desired to be within a centimeter cube at an 18 m standoff distance.

Target Engagement Requirements:	
Target tracking precision:	$\pm$ 10 μm
Tracking update rate:	~1 - few ms (~1 kHz)
Steering precision of driver beamlets on target:	$\pm$ 10 μm $_{rms}$ (rms for all beamlets)
Final steering time after glint:	~ 1-2 ms @ 100 m/s injection vel.
Injection accuracy:	$\pm$ 5 mm at 18 m

Table 1 - Preliminary target engagement requirements

The purpose of this thesis is to scale all components in the most prototypic way and first demonstrate engagement on a bench-top scale. The requirements are goals to strive for and keep in mind for the overall picture, while at the same time they help us realize and characterize present components to understand hardware, software, and physical limits.

At this point, the driver beam laser architecture has not yet been finalized for the actual power plant. We would like this engagement demonstration to be applicable to both the potential KrF (electron beam-pumped krypton-fluoride laser) and DPSSL (diode-pumped solid-state laser) driver beams to be used for the ICF power plant facility [4]. As it stands now, both driver systems will most likely use fast steering mirrors (FSMs) to steer their beams, so this engagement system will work for either driver beam architecture.

III. Target Tracking, Steering, & Engagement Tasks

III.1 Overview of Project

An overall view of the target engagement system demonstration is needed to give the reader an understanding of how each task contributes to the entire engagement system. References to unexplained terms and components will be described in detail later in this chapter.

Sequence of Steps for Target Engagement (see figure 5, 6, & 7 below):

1) Illumination laser emits a collimated beam.

2) Illumination laser overfills target, thus creating a Poisson spot on the CMOS camera some distance away.

3) Software analyzes the camera image and calculates the centroid of the spot; hence the target centroid is known.

4) Software commands the FSM controller to actuate the calibrated FSM in open-loop control to point the simulated driver beam onto the PSD (surrogate target.)

5) Any movement of the target by the target transport device is consequently corrected by the system, thus keeping the target illuminated.

6) The PSD is used only to verify correct open-loop illumination, as the real power plant will have no feedback except for the glint system firing ~1-2 ms before the target reaches chamber center.
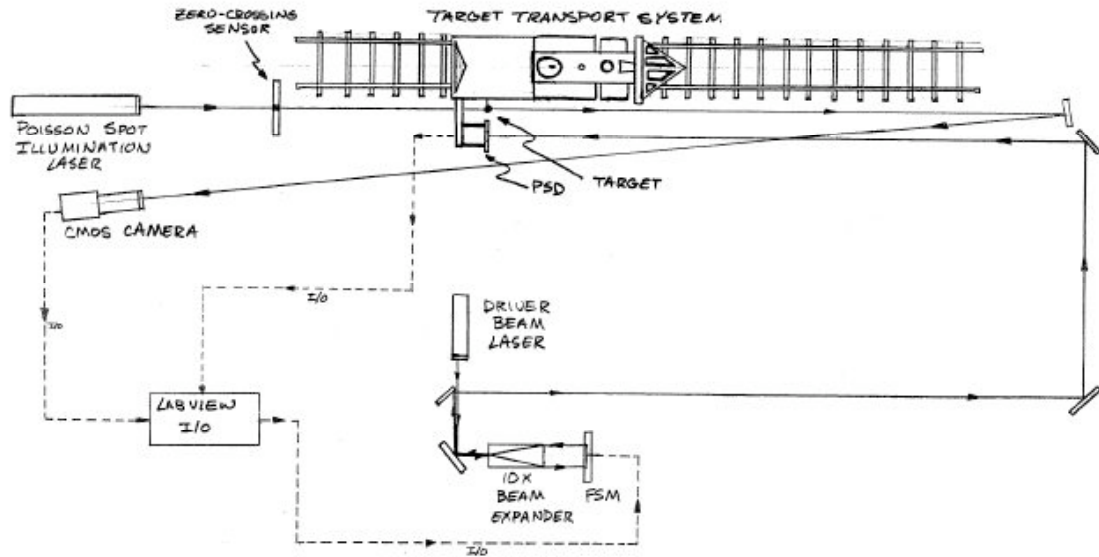
Figure 5 - Optical layout for target engagement demonstration (not to scale)
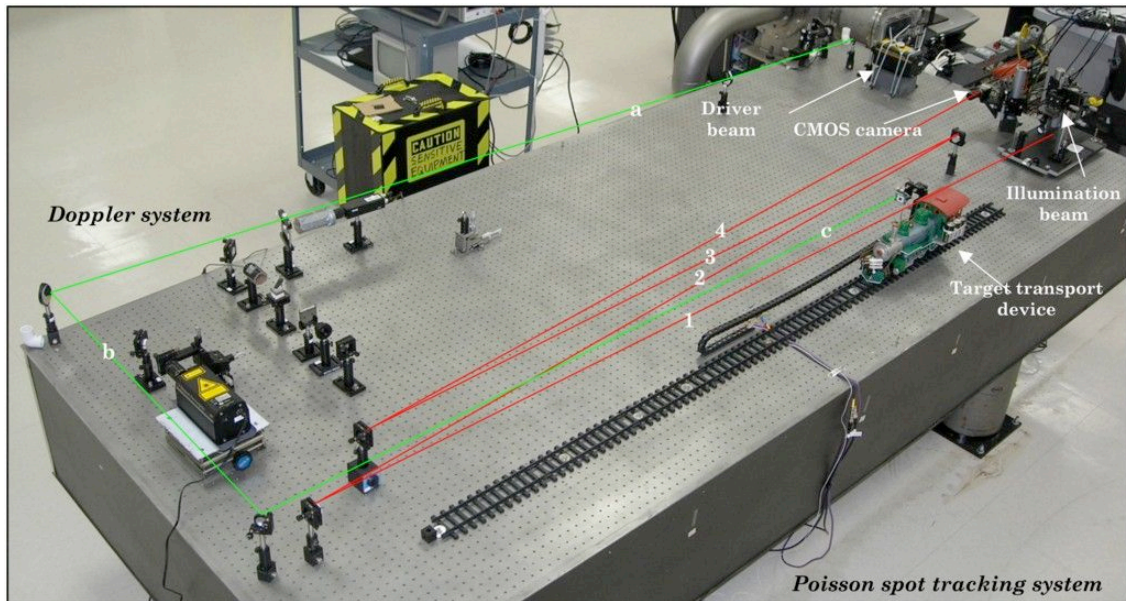
Figure 6 - Optical table showing Poisson spot illumination and driver beam lines with target transport device (R) and Doppler fringe-counting experiment (L)
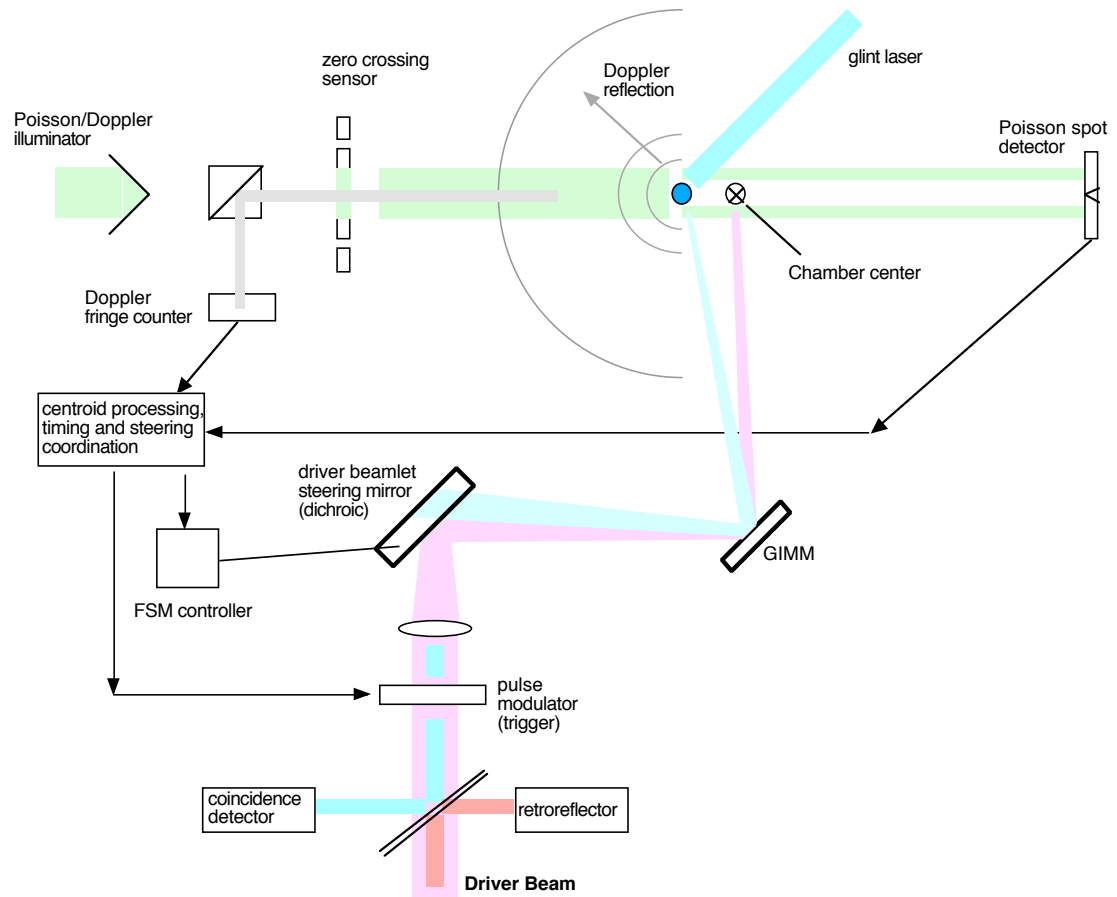
Figure 7 - Diagram of the complete integration of the target engagement R&D plan involving all subsystems/tasks

III.2 Overview of Tasks

The proposal for completing this thesis work has been divided into six individual tasks (1-4) with integration together in the final two steps (7, 9), as shown above in the R&D plan. Task 1 is the Poisson spot detection, task 2 is the driver beam steering demonstration, task 3 is the driver beam simulation, task 4 is the target transport system, task 7 is the active feedback from the Poisson spot and an integration of elements 1-4, and task 9 is a single beamlet, on-axis demonstration of tracking, steering, and engagement involving all the afore-mentioned elements.

IV. Poisson Spot Detection (Task 1)

IV.1 Overview of a Poisson Spot

The basic premise on how the target tracking system works employs a diffraction phenomenon known as the Poisson spot. A Poisson spot, also known as the Spot of Arago, is an intense diffraction pattern that occurs when a sharp-edged, circular obstruction (in our case, a sphere) is illuminated by a collimated Gaussian beam, such as that emitted from a laser. In the far field, the intense spot of light is exactly on axis with the sphere and exists at all points along the line of light. Additionally, as the distance from the sphere increases, the diameter of the spot increases and the intensity increases asymptotically reaching no more than the incident intensity (see figure 8 and 9). (A 4mm sphere casts a ~1 mm diameter Poisson spot at a target/detector distance of 10m; at 20m the spot is ~3 mm in diameter.) Furthermore, the diameter of the spot is inversely proportional to the diameter of the sphere, so a larger obstruction will cast a smaller spot.
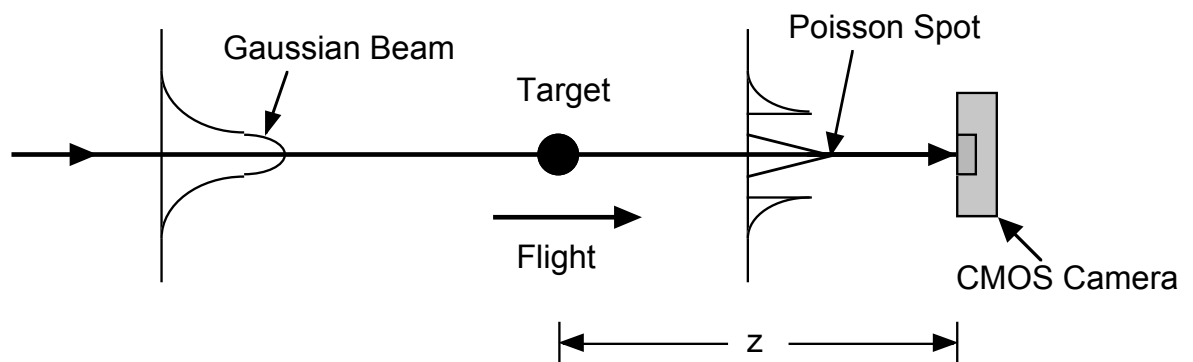
Figure 8 - On-axis Poisson spot creation and detection
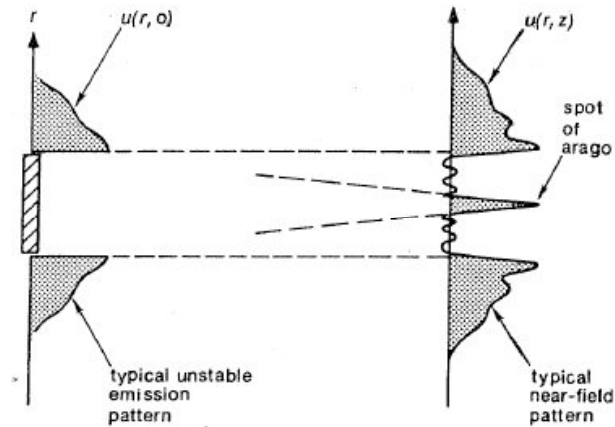
Figure 9 - The Poisson spot (R) imaged behind a circular aperture (L). Notice similar intensities between the incident light and the Poisson spot or spot of Arago. [11]

While the Poisson spot is mostly a nuisance to those who work with optics and photonics, we are using the spot to our advantage to capture and decipher centroid information from it. The general idea for tracking the target is to image the spot on a light-sensitive detector at the far end of the chamber on-axis to the flight of the target. Since the centroid of the Poisson spot is an exact representation of the centroid of the target, then the x and y position of the target can be determined to better than 10 μm for all locations from the target injector to the chamber center.

IV.2 Comparison to Other SLRs

It is of interest to compare our proposed tracking system with other straight-line-references (SLRs) that also use diffraction phenomena for alignment. The Stanford Linear Accelerator (SLA) is the premiere example of precise alignment over long distances using an SLR. The SLA uses 277 square Fresnel zone targets of different focal lengths to focus a laser beam onto a detector at the end of the chamber. They were

able to align the 3200 m long linear accelerator to ± 250 μm (accuracy of one part in ~5x10^{-8}) [9]. The Lawrence Livermore National Laboratory's Free Electron Laser (FEL) uses a retractable, sphere-generated Poisson line over 300 m to obtain ± 25 μm alignment accuracy (~8x10^{-8}) [10]. The FEL utilizes the Poisson line, which extends backwards through the center of the sphere and is perpendicular to the incident plane wave (see figure 10 below). Our IFE Target Engagement System uses sphere-generated Poisson spots to achieve an accuracy of ± 5 μm over 25 m (~2x10^{-7}). Our system uses the centroid of the Poisson spot to track the centroid of the target.
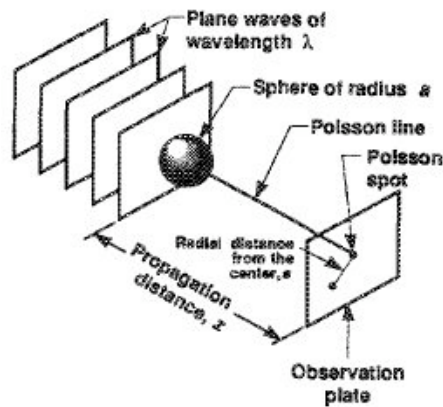
Figure 10 - The Poisson line is produced behind the sphere and extends perpendicular to the incident plane wave

IV.3 Verification of Poisson Spot to Theory

The aberration-free Poisson spot can be approximated by a zero-order Bessel function as explained in [7], [8], and [11]. Siegman shows that the intensity on or near the axis behind the obstacle is given approximately by:

$$\tilde{u}(r,z) \approx -\frac{\tilde{q}_o}{\tilde{q}(z)} e^{-j\pi N - a^2/w_o^2} \times e^{-j\pi N(r/a)^2} J_o(2\pi N r/a) \quad [8]$$

where r is the distance off axis, $\tilde{q}_o = J\pi w_o^2/\lambda$, N is the Fresnel number $(N(z) = a^2/(z-z_o)\lambda)$, λ is the wavelength, a is the radius of the obscuration, and w_o defines the width of the Gaussian beam. In [7], this expression has been evaluated for various values of the distance z when the radius of the obscuration r is 2 mm (expected target size), the width of the Gaussian beam is 4 mm, and the laser wavelength is 632 nm.
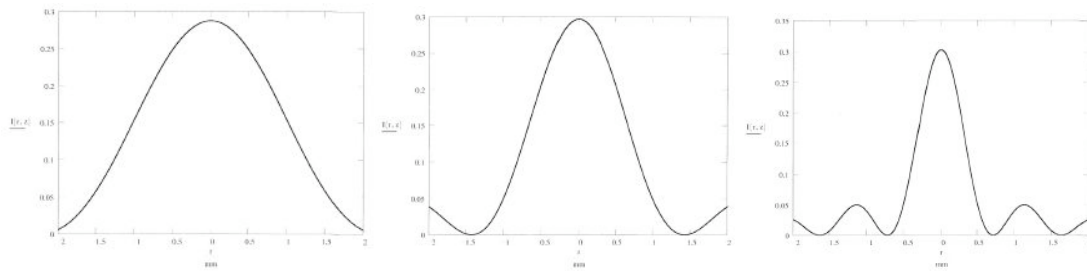
Figure 11 - Calculated Poisson spot intensity profiles at (L to R) 22 m, 14 m, 7 m [7]

Figure 11 shows the reduction in size of the FWHM (full-width, half-maximum) central spike as the z-distance decreases, i.e. the target travels toward chamber center. In the left-hand figure, the target-detector distance of 22 m represents the distance from the target injector to chamber center, the point at which the tracking system acquires and begins tracking the Poisson spot. At this range, the tracking precision is deemed to be larger than 10 μm, which is adequate for the purpose of large error-correction of the FSMs. The precision to which the centroid can be determined is based on the statement that when traditional thresholding and weighing techniques are applied to the encompassed area of the spike, the centroid can be determined to a precision of about 1% [7]. In the central figure, the target-detector distance of 14 m represents the distance

at which the target enters the chamber. Here, the tracking precision can be determined to 10 μm as the FWHM spike decreases (encompassing area decreases) and the centroiding technique is able to hone down on a more accurate reading. In the right-hand figure at 7 m, the target approaches the center of the chamber where fine-tuning of the FSMs is crucial. At this distance, the centroid can be determined to less than 5 μm due to a FWHM of 0.34 mm. The accuracy of these calculations will be confirmed as well as the exploration of the "dynamic diameter" of the Poisson spot as it travels from the injector to chamber center.

IV.4 Poisson Spot Detection

There are a few considerations required of the Poisson spot detector: it must be fast enough to capture the centroid of the spot in the required time (1 ms), it must have a large enough surface area to accommodate the range of movement of the spot (~5–10 mm), and it must be able to follow only the spot's centroid and no other areas of high intensity light. For example, a position-sensitive detector (PSD) is very fast (100's of kHz) and can track the centroid location of a Gaussian beam very accurately, but will fail in tracking a Poisson spot because the rings of incident light intensity surrounding the spot have a similar intensity as the central spot, as shown in figure 12 below. Therefore, as the target moves and surrounding rings from the spot move onto the PSD surface, the PSD will simply calculate the centroid of light intensity over the entire silicon ship, not the centroid of the Poisson spot. The spot could be imaged through an aperture at the PSD to alleviate this issue, but that would severely limit the range of movement. Similarly, a quad cell, which is divided into four equal regions and gives

voltages out depending on beam location on each surface, is excellent at keeping a beam centered, but fails at detecting a Poisson spot due to the similar intensities of light surrounding the spot.
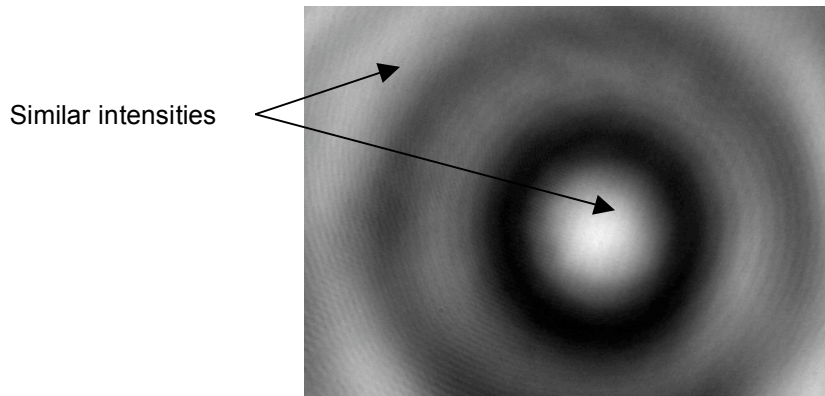
Figure 12 - Poisson spot imaged directly on CMOS chip showing similar intensities between spot and incident light around shadow's edge

These factors have led to the choice of a CMOS (complementary metal oxide semiconductor) camera to visually detect the spot. A CMOS chip is slightly faster than a CCD (charged-coupled device) chip because pixel functions and amplification are carried out directly on the chip itself, rather than on the adjacent circuit board, as done on a CCD chip. The speed of a typical CMOS camera is limited to ~100 fps due to the firewire (IEEE 1394) connection; a higher frame rate can be achieved by limiting the field of view, but again, the entire area of the CMOS chip is needed to give the largest viewable area possible. In other types of faster cameras, images are stored in flash memory for retrieval at a later time. These cameras may capture thousands of frames per second, but our tracking system requires streaming video to process the spot centroid in real time. For this low-speed demonstration, we chose a Basler A603-f

monochrome camera with a frame rate of 100 fps at 640x480 pixels (VGA resolution.) Each pixel is 9.9 μm square, which allows for centroiding capabilities to <5 μm, or half a pixel (more on this during software section.) A color camera is not needed since the image processing algorithms will only deal with gray scales and contract ratios. For the full-speed demonstration, a CMOS camera capable of 1000 fps at VGA resolution with a Camera Link interface will be used.

IV.5 Poisson Spot Illumination Beam

The Poisson spot illumination beam consists of a low-power (0.5 mW) helium-neon laser which is first expanded using a microscope objective, then collimated at a beam diameter of approximately 1.2 cm. The throw of the beam is ~10 m from the laser to the CMOS camera. The 4 mm target can be inserted anywhere in the beam, just as long as it is completely overfilled by the illumination beam. The resulting spot from the obscuration is imaged directly on the CMOS camera chip with appropriate neutral density filters in front to keep the chip from being saturated. Any movement of the target in 2D space is directly apparent on the 6.4 x 4.8 mm CMOS chip. One must be careful not to allow any laser light to reflect back into the HeNe laser cavity or else the resulting "mode-hopping" of the light interfering with itself inside it's own cavity will result in a flickering image on the camera.

For testing purposes, a 4 mm steel BB has been used since it is able to be held on the tip of a pin with a magnet, as shown in figure 13 below. Other forms of holding the target using glue, tape, and cement on a cover slide have yielded Poisson spots with greater obscurations.

4 mm steel BB

Poisson spot

laser beam

pin

magnet

resulting image with
Poisson spot in center
(image turned 90 degrees)
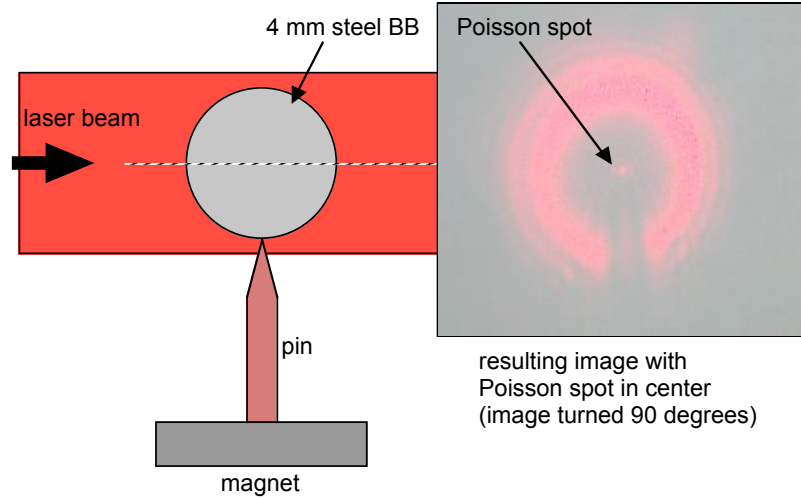
Figure 13 - Method of holding target on a pin using a magnet produces least-influenced Poisson spot

To disprove the perception that the obstruction must be opaque, DVB (divinyl-benzine) shells as well as glass spheres have been introduced into the illumination beam and both have created excellent, highly distinguishable Poisson spots. The target only needs to be a circular obstruction to produce a Poisson spot.

IV.6 Poisson Spot Verification

The Poisson spot was initially verified at multiple target-detector distances, including the three distances that were calculated in [7]. The spot was imaged in the NI's Vision Builder for Automated Inspection (VBAI) where the centroiding algorithm could be designed and optimized. As shown below in figure 14, a lineout was taken through the center of the spot to get the intensity profile.
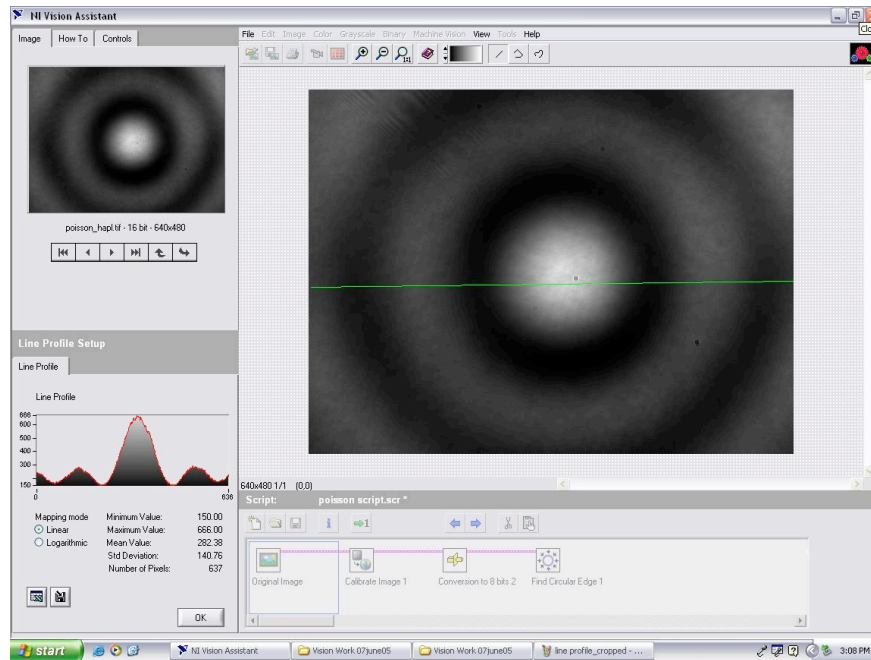
Figure 14 - VBAI screenshot with intensity lineout through Poisson spot

As shown below in figure 15, this intensity profile was confirmed, as expected, with the theoretical calculations, in this instance at a *z*-distance of ~10 m. From here, we could then proceed with finding the centroid of the central spike.
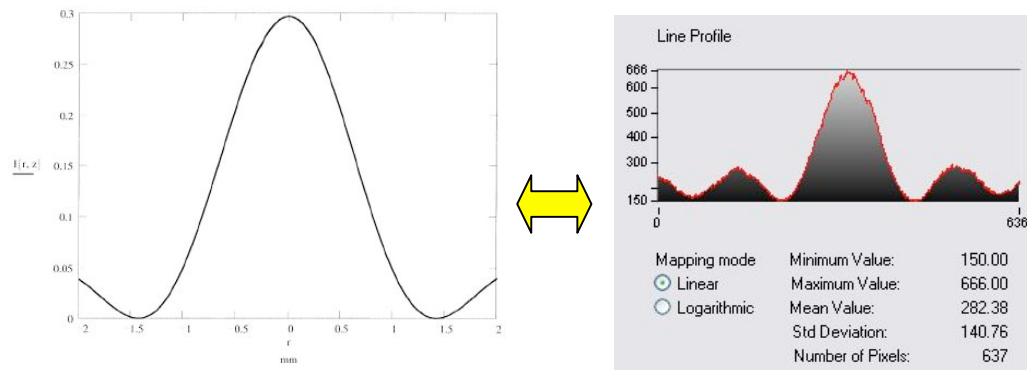
Figure 15 - Poisson spot intensity profile verification at a target/detector separation of ~10m with calculated profile (L) and actual profile (R)

IV.7 Centroid Calculation

Using a CMOS camera to detect the Poisson spot leads into the task of visually processing the image and determining the spot's centroid as fast as the camera acquires a new image. This is opposed to using a PSD or quad cell, which would give a direct voltage reading, corresponding to a displacement, of the beam movement. For the low-speed demo, we are using National Instruments' LabVIEW programming interface with Vision module and a multi-functional DAQ card to carry out centroiding calculations and I/O for different devices.

The main task of the software is to compute the centroid of the spot to a certain precision and time requirements. The centroiding algorithm must be designed to exclusively track the Poisson spot through the whole area of the CMOS chip and not be deceived by the incident light coming from around the edge of the target's shadow. It must also take into account the decreasing spot diameter as the target-detector distance decreases due to the target flying toward chamber center. Intuitively, the centroid-finding algorithm must be as streamlined and as fast as possible in order to keep up with the images coming in from the CMOS camera.

IV.8 Centroiding Algorithm

The first order of business was to design a centroiding algorithm with these goals in mind using VBAI. VBAI is useful in designing, testing, and benchmarking vision-based algorithms so that can later be imported into a full LabView program. VBAI was used to design and optimize the centroiding algorithm, which it calls "find circular edge." (VBAI uses static images saved to disk so the Poisson spots imaged

were not taken live from the camera.) The basis of this task is to draw two concentric

circles beginning at the near-centroid of the spot and specify the number of "spokes", or

search lines, which will be investigated, as shown below in figure 16. As a side note, the

saw-tooth edge on the right of the VBAI screen is a 1/4-20 screw that was used to verify

that the pixels were indeed 10 µm per side.
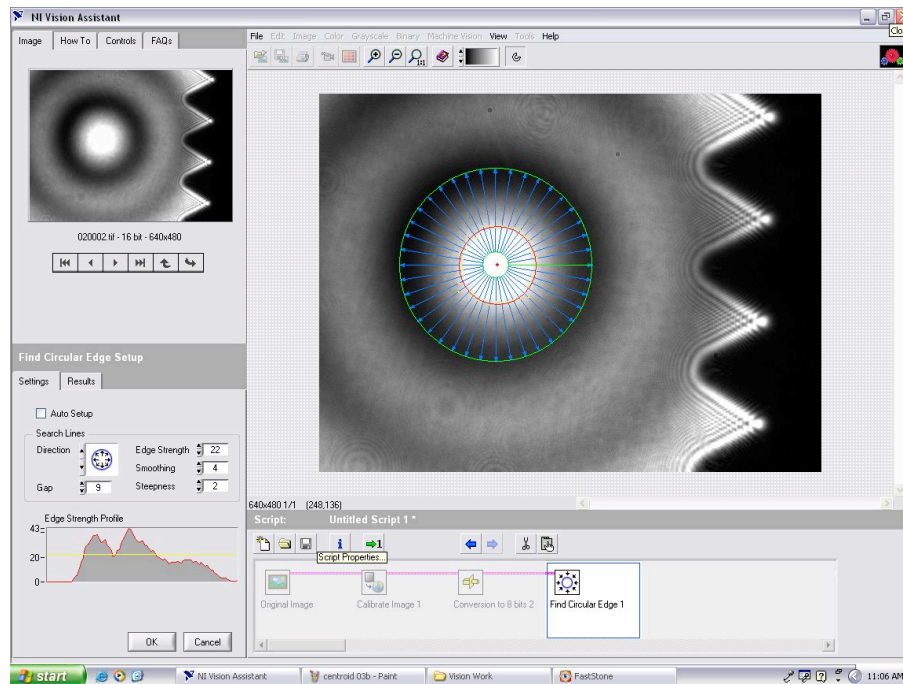
Figure 16 - Screenshot of Poisson spot centroiding spoke optimization. Saw tooth edge on right is a 1/4-20 thread used to verify pixel size.

The software searches along the entire one-dimensional spoke length, pixel by

pixel, while employing filtering to reduce the effects of noise. It computes the edge

strength (contrast) at each point and compares it to the user-specified values of edge

strength, smoothing, and steepness. Figure 17 below shows the edge detection

technique, based on the user inputs, which chooses the grayscale contrasting gradients and picks the edge location as the midpoint between the two contrasts.

| 1 | Pixels | 3 | Width | 5 | Contrast |
| 2 | Grayscale Values | 4 | Steepness | 6 | Edge Location |
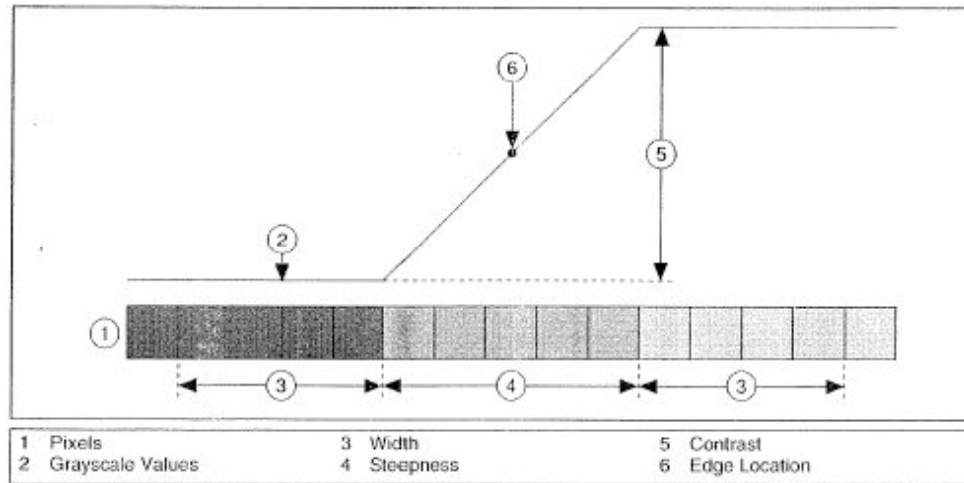
Figure 17 - Centroiding algorithm's edge detection technique [12]

Using this systematic approach, the edge location is determined along each spoke and a circle emerges along the edge of the Poisson spot, approximately at the FWHM location. Figure 18 below (two PS pictures) gives a clearer depiction of this edge-determined circle. From here, the centroid average of this circle can easily be determined in terms of the number of pixels from the top-left of the camera chip. A more in-depth discussion of NI's edge detection tools can be found in their Vision Concepts Manual [12].

IV.9 Spoke Optimization

There is a tradeoff between speed and precision of the edge detection algorithm depending on the number of spokes used to compute the centroid. A study was done on

a saved Poisson spot image to determine the optimal tradeoff between the two. Number of spokes from 360, 72, 36, 18, 12, 8, and 6 were tested and plotted with their computational time against their standard deviation of the centroid position. The optimal tradeoff was found to be 12 spokes which gave a standard deviation of 4.6 μm (within our error budget) and a computational time of ~0.7 ms on our Dell PC. The specified inputs and number of spokes were subsequently used in further testing of the target engagement system as the best combination of speed and precision.
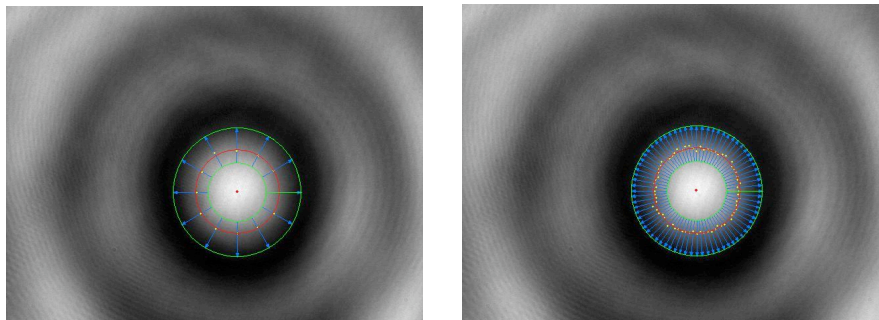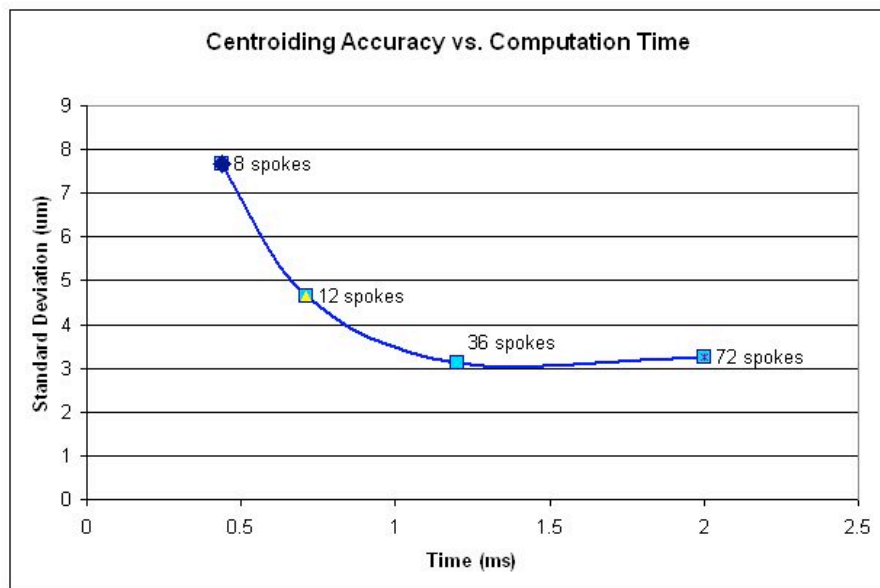
Figure 18 - Centroiding spoke optimization graph. Bottom-left: 12 spokes. Bottom-right: 72 spokes

IV.10 Additional Image-Processing Steps

Determining the centroid is the key task in the overall image-processing algorithm. However, as shown in table 2, more steps are required to output the x, y coordinates of the target's centroid.

LabView Algorithm Timing Breakdown per Frame (1 of 2)	Approx. Time (ms)
Image Processing	
Initialize/setup visualization sub-vi's with specified parameters (1st loop)	0.5
Capture image from 100 fps CMOS camera via firewire card	6
Search image and match Poisson spot pattern with one saved in memory	9
Set coordinate system to center of matched pattern	0.5
Find circular edge of the Poisson spot using specified parameters	0.5
Output centroid coordinates with pass/fail boolean, convert from pixels to distance from CMOS chip center	1

Table 2 - LabView algorithm timing breakdown for image processing only (1 of 2)

First, the entire image-processing program must be initialized with the user-specified parameters of detecting the edge of the Poisson spot. Other initialization procedures include setting up the camera, adjusting the brightness, shutter speed, and gain, erasing the previously saved results in memory, resetting the image frame number, and a check on I/O devises that the program will utilize. The camera is initialized in format 7, mode 0, with a pixel range of 656x491, and a packet size of 4092, which allows for maximum data transfer through the firewire bus. All these initializations take approximately 0.5 ms to get ready.

The firewire camera is then triggered at 100 Hz and the resulting image is streamed to the computer in about 6 ms. A shorter firewire cord will result in a faster downlink time from the camera to the firewire bus.

The image, now in the PC computer's memory cache, is ready for image processing. The pattern-matching tool is used to measure the similarity between an idealized representation of a feature (the Poisson spot), and a similar feature that may be present in the image. Using the technique of cross correlation [12] [13], the algorithm searches the entire pixel range of the CMOS chip for a similar-looking Poisson spot to the one it has saved in memory. It then ranks the match on a percentage scale and the user-set threshold (60% similarity for a pass) determines whether it passes or fails. A pass/fail boolean indicator on the front panel of the LabView screen relates whether or not the software found a successful match. This part of the image processing sequence takes approximately 9 ms to complete using a coarse search method.

Although this method of searching the entire CMOS chip for the spot is computationally intensive, it is needed since the spot can move over the entire range of the chip. It may seem that simply looking for the most intense spot would be enough to find it, but when the spot is at the extreme edge of the chip, the incident light coming from around the target is also imaged on the chip as well. An algorithm that searches just for the greatest intensity will fail at finding the real Poisson spot in this situation. (See figure 12 above, which shows the similar intensities).

One point to note is that the match pattern algorithm can only maintain the 5 μm location precision for a target range of ± 2 m from where the Poisson spot image was saved from. This is due to the changing diameter of the spot as the target is translated in the axial direction. Outside this range, the centroid can still be found, but the precision cannot be guaranteed to 5 μm.

The next step in the image-processing algorithm is to set a coordinate system to center of matched pattern. This coordinate system will serve as the approximate centroid of the Poisson spot and therefore the starting point for the circular edge algorithm. This step takes ~0.5 ms.

Finding the circular edge is the next step that must be done, as described above in the centroiding algorithm. The two concentric circles originate at the origin of the temporary coordinate system and the donut of spokes radiate from there. The information gained from the circular edge detection provides the coordinates of the centroid of the Poisson in approximately 0.5 ms.

The last step in the image-processing algorithm is to output the centroid coordinates to the main LabView program where they are converted from pixels to a distance from the center of the CMOS chip. The coordinates are also plotted on an x,y graph to visualize the Poisson spot movement and the tracking by the driver beam. This step takes about 1 ms to perform.

It should be noted that the image-processing algorithm running in this configuration is not deterministic; in other words, the time it takes for completing the image processing is not specifically known. The CPU of the computer is multitasking with other programs and Windows tasks, so the image processing is not given absolute priority on the processing chip. This makes the algorithm run without determinism, but is necessary for R&D purposes and ease of user-programmability.

IV.11 Next Generation Vision Algorithms

The next generation system will likely aim for 1 ms cycle time per update. Such a 1 kHz system will either run on an extremely fast real-time operating system or have dedicated image processing chips with a "hard-wired" algorithm to be fully deterministic. Next generation algorithms may employ thresholding techniques to only stream pixels from the camera whose intensities exceed a given threshold value. This will limit more pixels from coming off the camera, and thus there will be fewer pixels that need to be processed by the CPU. Binning is another technique that may be used to reduce the number of pixels. This method groups adjacent vertical and horizontal pixels and averages their intensity values, thus increasing the signal to noise ratio and the sensitivity of the camera, but also decreasing resolution.

One method to place and reduce the region of interest is to use a fast (photo-sensitive detector) PSD to get the general location of where the Poisson spot is to within a hundred microns. This general centroid can then be used to adjust the position and size of the ROI of the camera, thus keeping the ROI as small as possible. Still another method of reducing the effective ROI is to inject the target more accurately into the chamber. The ROI on the CMOS chip can be reduced since the target will not be wavering as much. Additionally, the decreasing size of the Poisson spot as it travels closer to the detector may be a potential means of approximating the axial position of the target depending on the spot's diameter.

IV.12 Beam Stability

One problem we encountered early on while imaging Poisson spots was a constant wavering of the PS on the CMOS camera. The centroiding algorithm would clearly show the PS randomly wavering up to 70 μm. While some error is associated with the centroiding algorithm itself, this was unacceptable. The hypothesis for the wavering (and the correct one) was that the air conditioning in the building was producing substantial air currents of varying density over the optical table, thus disrupting the beam and causing it to waver. A simple solution was to build a tent structure out of PVP pipe and cover it with a sheet of plastic. This solution worked very well and the still air inside the tent decreased the beam waver seven times its nominal disruption. See appendix figures 34 and 35 for supporting graphs.

V. Driver Beam Simulation (Task 2)

V.1 Driver Beam Overview

The IFE power plant's driver beams will all converge on the flying target as it approaches chamber center and will release ~50-60 kJ joules of energy each in an 8 ns pulse on the target, thus imploding it and compressing it to one thousand times its nominal density [14]. The power plant will introduce 60-70 driver beams onto the target, depending on the layout of the power plant and the geometric constraints of introducing a uniformly spaced array of beams onto a sphere [15]. Each beam path will be a few hundred meters long and will be composed of 50 beamlets which all run along angle-coded internal paths [15]. This means that there are a total of 3,000 beamlets that need to be aligned so they all converge on the target exactly at chamber center.

We plan to scale the optics for this project accordingly to accurately simulate the full-scale power plant driver beams, but without amplification. The optics will be scaled to allow a smaller diameter beam to travel over a shorter distance while retaining similarity in the magnification, diffraction limit, beam throw, etc. By using small, low-power optics, substantial cost savings are possible while achieving a functional demonstration.

Task 9 dictates two demonstration steps: on-axis and off-axis engagement. The on-axis demonstration is deemed easier because it decouples the z-axis position requirement from the Doppler fringe-counting system, which is needed for timing the off-axis steering. For task 9a, the driver beam shines on-axis to the motion of the target, which is located on the target transport device. With regard to the driver beam profile, it is required that the beam be collimated the entire length of the target travel – if it is

focused to a point, then the target will pass into and out of that point and the driver beam diameter will vary according to the z-axis position. A collimated beam will allow for a demonstration of a continuous tracking and engagement system along the entire path of the target transport device range (~2m). For a real reactor, however, the driver beams will all be focused on a small area in space that the target will pass into. For task 9b, the beams will utilize z-position position and velocity data acquired from the Doppler fringe-counter to steer their focused beams onto the target as it passes into chamber center.

V.2 Translating Aperture, Fast Steering Mirror

We initially planned to scale down and simulate the KrF driver beam by using an incoherent light source and a simple optical train with approximately 10:1 magnification, modeled after the amplified ASE source in Lehecka's description of the Nike laser system [16] and McGeoch's schematic of the amplifier front end [17]. In this layout, either a translating aperture or fast steering mirror can be used to steer the driver beam onto the target. Work was done on the feasibility of translating an aperture to steer the beam and it was concluded that an aperture could indeed steer the beam, with resolution depending on the magnification.

In recent months, however, the emphasis has been placed on using a FSM for both the KrF and DPSSL driver lasers because relative rotations of the beams (with respect to one another) as they propagate through different beamlines will result in inaccuracies if aperture steering is used. Additionally, the optics would need to be oversized because relaying a beam causes the beam paths to move laterally. Therefore,

the aperture steering idea was deemed a backup option and FSMs were considered to be the primary beam steering method, regardless of the driver beam chosen. As a result, the simulated driver beam's incoherent light source was converted to a 0.5 mW helium-neon (HeNe) laser for simple target illumination. After experiment with different lens/beam-splitting cube configurations and losing too much power to properly illuminate the target, the following configuration was set up to image the simulated driver beam onto the target as shown below in figure 19.
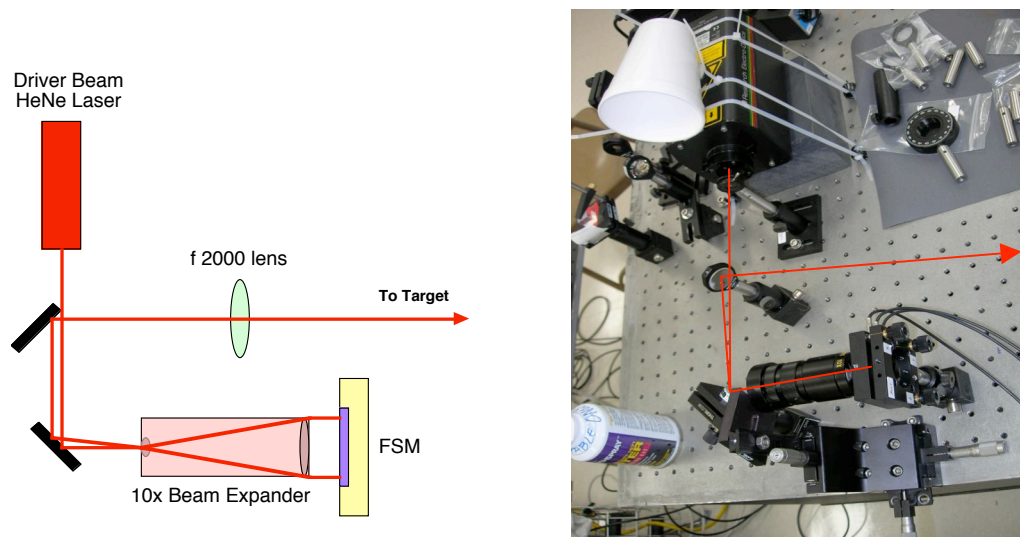
Figure 19 - Optical layout and diagram for driver beam simulation with FSM

V.3 Current Driver Beam Configuration

The HeNe beam is directed into a 10x beam expander onto the ThorLabs FSM. After being steered, the beam is reflected back through the beam expander, which effectively multiplies the throw of the FSM by ten times in order to achieve significant angular throw. The beam is then directed through a half-diapter lens obtained from an

optometrist (essentially a f2000 mm focal length lens) that is placed at the effective focal plane of the FSM/beam expander. This configuration permits the beam to behave telecentrically from the lens to the target and produces an effective steering throw of 6 mm on the target. In other words, the driver beam is collimated and parallel from that lens onward. The spot size on the target is ~2-3 mm due to the divergence of the beam over the ~2.5 m from the laser to the f2000 lens, and the telecentric throw from the lens to the target is ~6 m. This is not exactly prototypic in size, but the telecentricity of the beam is deemed more important for the on-axis demo.

V.4 Beam Zooming

In the proposed power plant, the driver beams will be "zoomed" during operation, meaning the laser focal spots will shrink in steps as they follow the compressing target. It has been shown that this method of following the compressing target can boost laser absorption substantially (30%) over the time of the pulse [14]. However, the target engagement R&D plan is not yet developed enough to propose driver beam zooming, although it must be considered for future integration.

VI. Beam Steering Demonstration (Task 3)

VI.1 Steering the Beamlets

The subject of steering the driver beams with FSMs was mentioned briefly above in the discussion of simulating the driver beam optical train. This section delves deeper into how to steer the driver beamlets to hit the target to within ±10 μm rms with a final steering input 1-2 ms before the target is lased. Each of the 3,000 beamlets will have its own FSM and each one needs to be pointing exactly at chamber center, as well as be aligned with one another, right before the driver beams fire. The large final optic, called the grazing-incidence metal mirror, or GIMM, will be stationary, so the actual beam steering will be done further upstream, approximately 20 - 30 m away, as shown below in figure 20. Steering a large optic such as the GIMM is very non-trivial due to the weight, size, and moment of inertia of such a large mirror (3.25 m x 3.00 m).
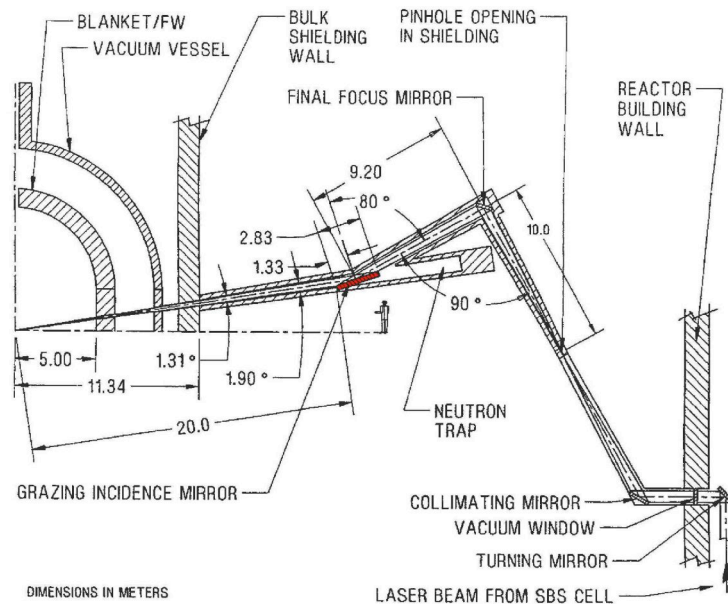

Figure 20 - Placement of the GIMM, FSM, and final optics in the proposed IFE power plant [2]

VI.2 Actuation & Steering Means

As mentioned in the driver beam simulation section, we initially considered using a translating aperture driven either by piezoelectric actuators, voice coils, or stepper motors. Stepper motors proved to have a long range of motion but were too slow due to their mechanical screw drive and therefore not an ideal solution for our application. Voice coils, most commonly known for their use in speakers, have ranges of motion on the millimeter scale and are able to operate at high frequency, but their response time is on the order of milliseconds – we require the final steering input to accelerate, move, and settle the mirror in 1-2 ms. Lastly, we examined piezoelectric ceramic crystals which operate using the piezoelectric effect where an applied electric field on the crystal induces strain proportional to that field. PZTs have excellent response times in the microseconds range and they are as precise as the voltage (usually 0-100 volts) resolution driving them, typically in the sub-micron range. Their elongation length is proportional to the height of the crystal stack – usually a stack can elongate 1% of its height at full driving voltage. PZTs integrated into a tip/tilt mirror platform typically have 2-4 mrad range and sub-mrad resolution, which is essential when the beam is thrown 20 meters.

We have assessed different steering means of actuating a small (~1 in.) mirror to meet our demonstration speed and precision requirements. Many companies such as Newport, ThorLabs, Piezosystem Jena, Physik Instrumente, Bell Aerospace, and Axsys Technologies offer off-the-shelf fast steering mirrors with kilohertz bandwidths and microradian resolutions. Our initial steering demonstrations have utilized a ThorLabs 1-inch FSM. By working with this FSM and characterizing its frequency response, we

have exposed certain limitations of its design, which has helped us to realize the need for a higher-quality piezo-actuated device.

VI.3 Beam Steering Demonstration

A controller, which amplifies the input voltage of 0-10 V by 15 V/V, drives the PZT actuators in the FSM. At full input, the ThorLabs FSM tilts approximately 1 arc sec, thus giving a ~300 μm beam throw at a meter offset. By imaging the driver beam through the 10x beam expander, as shown above in figure 19 above, the throw is increased to 3 mm at 1 meter, or 6 mm at 2 meters. This allows the beam appropriate engagement flexibility through the telecentric lens configuration.

The on-axis beam was calibrated by running the FSM controller through its range of input voltages and observing the deflected beam on a position sensitive detector (PSD.) The LabView program could then reference this fairly linear gain curve and steer the FSM in open loop using the observed position of the target's Poisson spot. See appendix figures 36 and 37 for an example of the PSD displacement to FSM voltage gain curves.

To verify accurate target illumination of the steered beam for the slow dynamic demo, we fixed a PSD a set distance from the target, as shown below in figure 21. The PSD outputs a set of vertical and horizontal voltages of the centroid of light incident on the PSD chip. (The PSD must be calibrated as well for different sizes and intensities of beams imaged on it.)
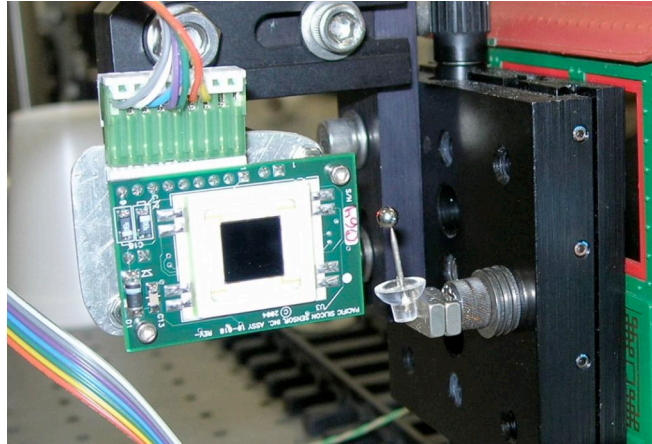
Figure 21 - PSD at a set distance offset from the target, used for driver beam accuracy verification

The PSD does not feed back the driver beam's position to the control program but rather is simply a verification tool. The ultimate target engagement system is inherently open loop with no feedback except for the final correction provided by the glint system immediately before the driver beams fire. The PSD simply shows the ability of the FSM to accurately illuminate the target in motion and it gives an indication of how well the calibration curve has been set for the FSM. In figure 22 below, a graph is given showing the displacement of the Poisson spot detected by the centroid algorithm along with the driver beam's position on the PSD, i.e. target. This illustrates how the tracking system detected the PS's movement and steered the beam to maintain the same position on the PSD/target. Ideally, on the graph below, the "driver on PSD" should not move, which would mean the calibration was exactly compensating for the target's movement.
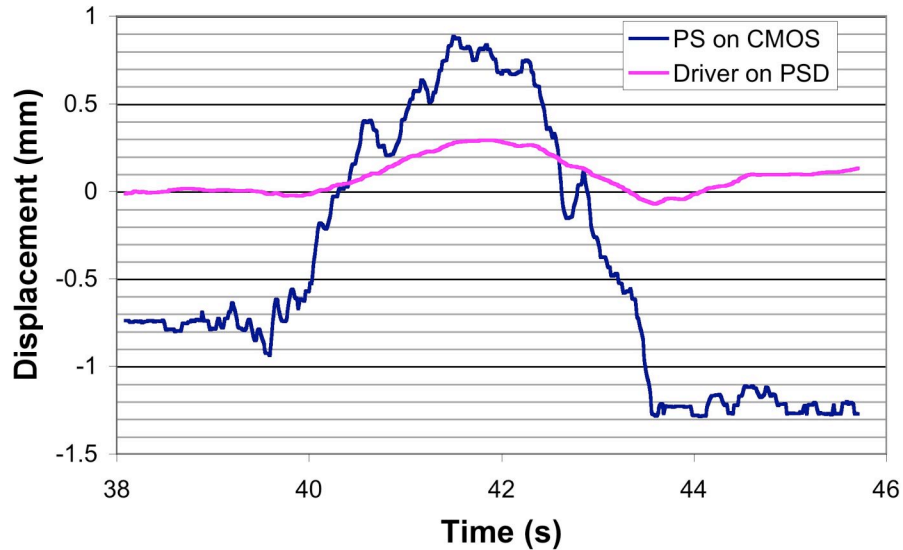
Figure 22 - Open-loop beam steering from PS centroid data (driver beam on PSD should not move)

The simulated driver beam in use now is a continuous-wave HeNe that tracks the target continuously as it travels along the target transportation device. Sometime in the future we would like to simulate the actual 8 ns pulse of the driver beam with a pulsed or chopped laser. The laser would be capable of physically marking a plastic target to confirm correct target illumination and engagement. Such an addition to the driver beam system will require significant timing coordination between the firing of the laser, injection or transport of the target, and target velocity/position measurements.

VI.4 ThorLabs FSM Characterization

The ThorLabs FSM used for this beam steering demonstration is a relatively inexpensive fast steering mirror with a limited range of motion. This FSM was used simply because it was available and easily accessible. After working with it for some time, we began to notice limitations in its design, especially at high frequency

modulation. From the beginning, we had some qualms regarding the mounting of the mirror into the FSM frame. The mirror rests against two nylon supports while the third point is tightened down on the mirror with a set screw. The mounting situation looked feeble and compliant for holding a FSM optic, so we decided to do a simple step and frequency response characterization to quantify its motion characteristics. A picture of the FSM and the characterization block diagram are shown below in figure 23.
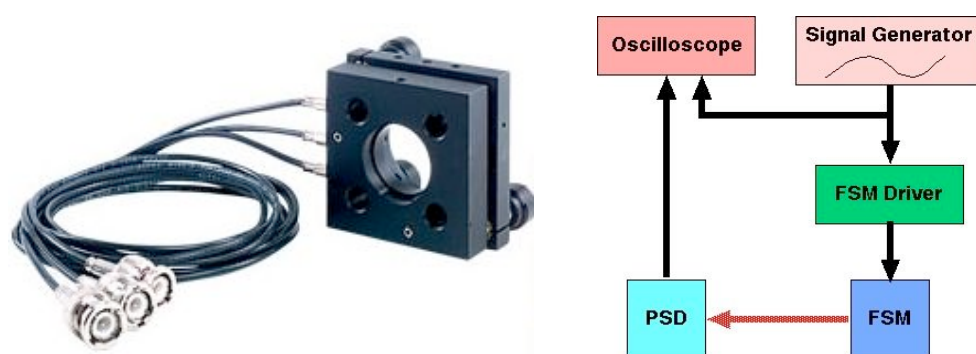
Figure 23 - ThorLabs FSM with one-inch optic (L) and characterization block diagram (R)

A signal generator outputted a 5 V step (half the allowable FSM voltage) to the FSM controller, which subsequently gave one of the piezos a 75 V step. The FSM then steered the beam on the PSD and the resulting movement was captured. The step response is shown below in figure 24 and confirms a substantial overshoot and a settling time of more than 60 ms, which is an unacceptably long time. This is most likely due to the compliance in the mirror's mounting supports and the kinematic mount arrangement.
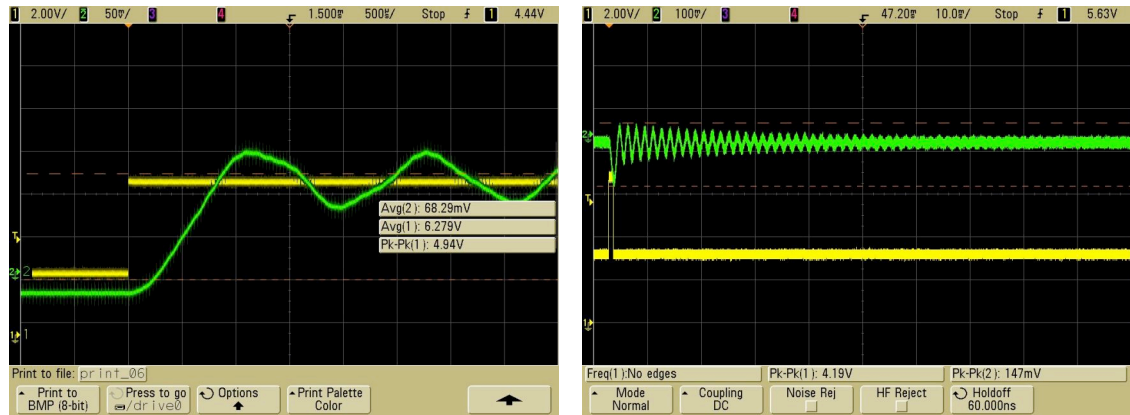
Figure 24 - FSM step response illustrating long settling time

Additionally, we performed a frequency response analysis for the FSM by inputting a range of voltages into the controller through a range of frequencies. As shown below in figure 25, the mirror has two distinct resonance modes at ~620 Hz and ~1.3 kHz where the beam resonates at dangerously high amplitudes. This first mode is fairly low for a FSM and very obtrusive when requiring inputs around that frequency. Comparably sized 1-inch FSMs, such as from PI, have their first resonant mode at 2.4 kHz. Again, this test helped us better understand the characteristic response of our FSM and emphasized the need for a better, higher-quality (where the mirror is epoxied to the tip/tilt platform and this platform is suspended on flexures) FSM for the next generation of beam steering.

Frequency Response Curve of FSM
R (Vpp input/Vpp PSD) vs. Frequency
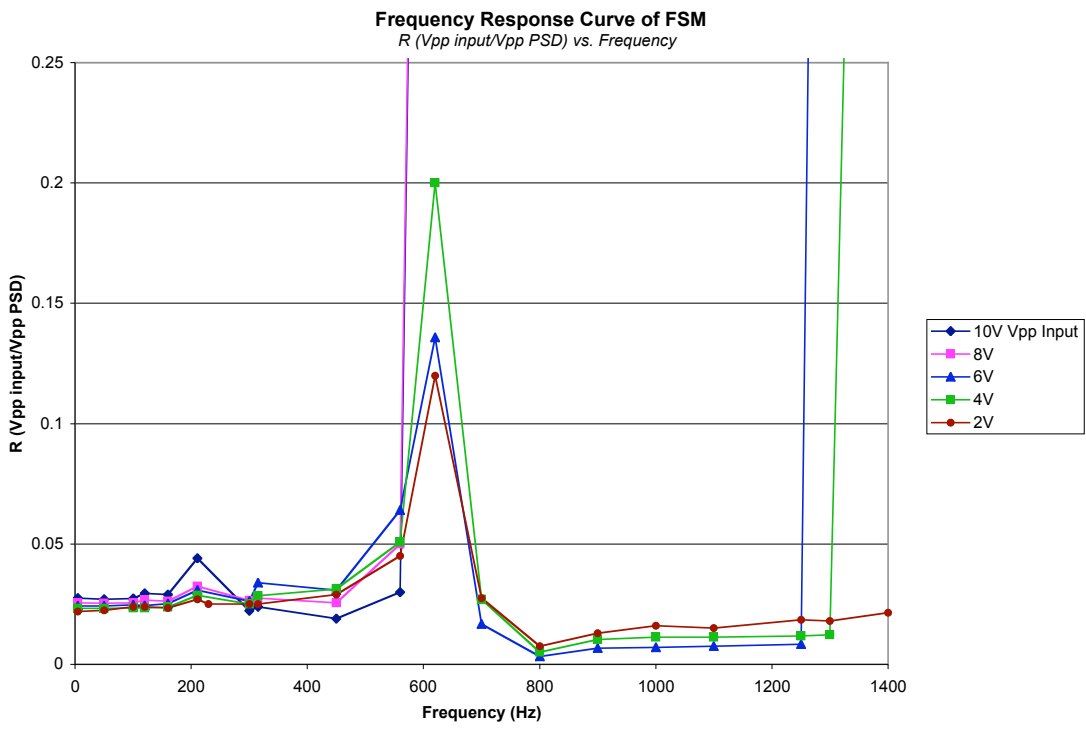
Figure 25 - FSM frequency response at increasing drive voltages illustrating two distinct resonance

modes

VI.5 Additional Algorithm Steps

The majority of the target tracking LabView algorithm time is spent doing the image processing, as described in the Poisson spot detection section above. However, the time for reading and writing the data acquisition (DAQ) channels, converting voltages to distances, and controlling the FSM must also be accounted for. The following table 3 breaks this timing down.

LabView Algorithm Timing Breakdown per Frame (2 of 2)	Approx. Time (ms)
Read DAQ Channels	
Read DAQ channels for PSD voltages, convert to distance, graph, display	2
FSM Control	
Apply FSM open-loop control algorithm gain to x & y axies and convert pixels and voltages to distances	1
Write DAQ Channels	
Output gain voltages to FSM controller; graph and display actual and desired driver beam location on front panel	2
FSM mechanical response time	1

Table 3 - LabView algorithm timing breakdown for read & write DAQ commands, FSM control (2 of 2)

During one loop of the tracking algorithm, the DAQ channels must be interrogated for the two PSD voltages corresponding to the centroid of the driver beam. These voltages are then converted to distances using the calibration curve as described above. For informational purposes, the centroid of the PSD is graphed and displayed on the front panel, as well as the PS centroid. The PS is expected to wander about, but the driver beam should remain fixed on the center of the PSD. The program then sends the appropriate gain (0 - 10 V) to two DAQ output channels to input to the FSM controller. As well, the mechanical response time to the voltage input must also be accounted for. The combination of these I/O steps takes ~6 ms.

VI.6 Transition from Poisson Spot Tracking to Glint Alignment

As the power plant is in operation, the beamlets are thought to likely "drift" out of alignment from the previous shot, thus exceeding their error budget of ±4 μm [18]. The amount of drifting of the beamlets is not readily known as of now, but is thought to be caused by a host of influences including the motion of the mirrors, the vibrations in

the optical train, and the fusion reaction itself taking place inside the chamber. This calls for a reference system that needs to be established immediately before the driver beams fire. Flint proposes such a "glint" system that uses the target itself as the point of reference to fine-tune the beamlets 1-2 ms before it enters the chamber center [3]. He proposes two different scenarios, one optimistic, the other pessimistic, depending on the assumptions used. This thesis does not involve demonstrating the glint alignment system, but it resides in the R&D plan for consideration and eventual integration.

The target tracking system is an open loop except for one data point from the glint system immediately before chamber center. This means that the location at which the beamlets are all pointing is set with a calibration curve for that specific FSM location so each FSM will have a different calibration curve. The accuracy to with which the beams have been steered during the first 100 ms is not verified until 1-2 ms before the driver beams fire. From the target injection to this point, the FSMs will have time to do rough positioning and make large corrections toward the anticipated implosion point. Right before the lasers fire, the glint system will give a final point of reference of the target itself, and all FSMs will do a final quick adjustment to position themselves accordingly. The "handoff" from the coarse adjustment Poisson spot tracking system to the fine adjustment glint alignment system will take place right after the last centroid update with enough time given for the glint laser to fire. The glint alignment will take precedence over the PS centroid information.

VII. Target Transportation Methods (Task 4)

VII.1 IFE Power Plant Target Injection

In the IFE power plant, the 4 mm diameter target is injected into the chamber with a velocity greater than 50 m/s. This minimum injection speed depends on the radius of the chamber and the repetition rate of the injected targets, as well as the anticipated clearing time of the gases and debris of the fusion reaction from the preceding target [18]. The accuracy required of the injector is ±5 mm at a standoff distance of 18 m. A more accurate injector will lessen the requirements on the tracking system in terms of searchable area and algorithm speed, as well as the distance the driver beams must be steered. In a separate yet relevant experiment, electromagnetic steering of a charged target immediately after injection hopes to steer the target to higher accuracy into the chamber center.

The target will most likely be injected vertically to negate the effects of gravity induced when firing from a horizontal position. Possible methods of injecting the target include acceleration with a light gas gun, a mechanical injector, and an electromagnetic injector. Regardless of the injections means, the target must be tracked along its axial position all the way from the injector to the chamber center. Means of introducing a collimated laser beam (required for PS tracking) behind the target's path of travel are investigated. If a mechanical injector or gas gun is used, then there is necessary equipment in the axial line of sight of the target, thus making it difficult to introduce a beam down the same path. Such means of injection, as well as vertical injection, will require a tilted rotating mirror with a hole in it that will allow the target to pass through, and then rotate to permit the beam to have an unobstructed view of the flight path. An

electromagnetic injector, however, does not require any equipment along the axial path of the target and will allow the illumination beam full access to the flight path. See figure 42 in the appendix and [7].

VII.2 Micron Stage & Beam Train

We initially translated the target on a micron-precision stage, held in place with a magnet as shown below in figure 26 and above in figure 13. The stage was necessary to confirm the accuracy of the Poisson spot detection system and the centroiding algorithm. After these were verified, we searched for another means of transporting the target a longer distance with less determinism. Eventually we employed the use of an electric train with a variable-speed controller. The slightly uneven plastic track running 2 m along the optical table provided a longer distance and higher speed platform (few cm/s) with which to track the target and improve the Poisson spot tracking algorithm. The "beam train" also provided a stable platform to mount the PSD to for driver beam verification purposes.
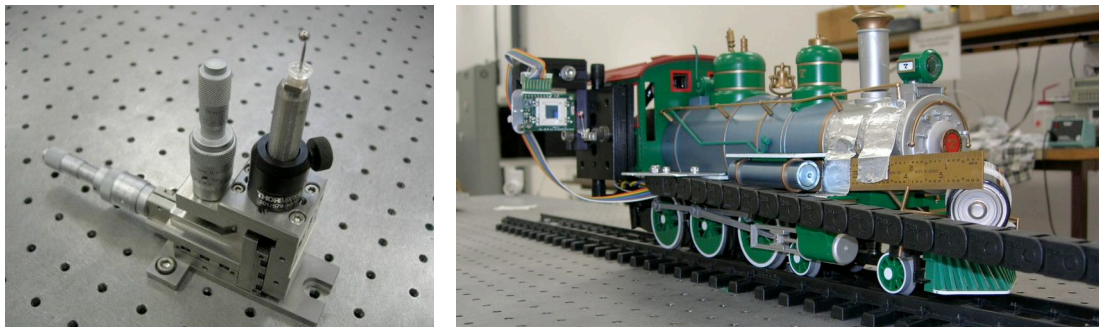

Figure 26 - Target translation methods using a stage (L) and a beam train (R)

The beam train was used exclusively for some time until the need arose for a more prototypic way of moving the target as if it were injected into the chamber. The new target transportation system needed to have speeds in the meters-per-second range and follow a parabolic trajectory most likely to be displayed by a power plant target.

VII.3 Air Rifle Injection

One avenue we looked into was firing a pellet in the target injector system at General Atomics. We used a very accurate FWB Feinwerkbau Model 603 Olympic-grade air rifle (.177 caliber) with a muzzle velocity of 170 m/s (single pump-lever action) and accurate to < 1 mm at 20 m using a 10x scope. See figure 27 below.
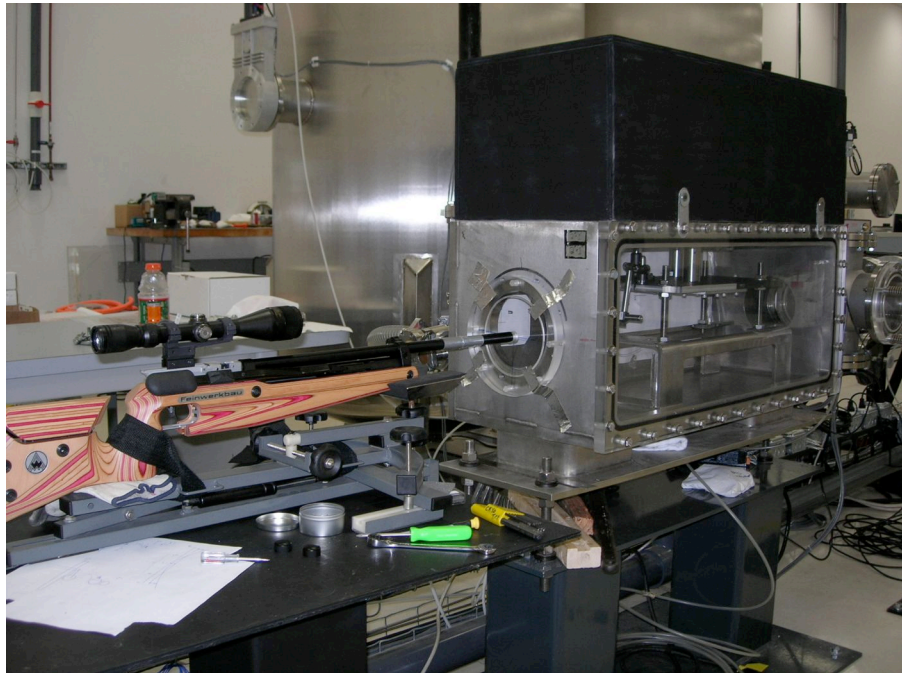

Figure 27 - FWB rifle firing into injector chamber for high-speed tracking

The Poisson spot illumination beam was introduced into the chamber immediately above the rifle's barrel by a 45° mirror and then propagated down the injector and out to the CMOS camera by another 45° mirror. The rifle was aimed slightly below the final 45° mirror located at chamber center. The lead pellet assumed a flight trajectory that took it 20 m to the chamber center with an apogee of 2.2 cm occurring half-way down. See figure 28 below. A pellet was chosen over a BB for its better flying characteristics and a Poisson spot could still be imaged from the circular obstruction of its skirt.
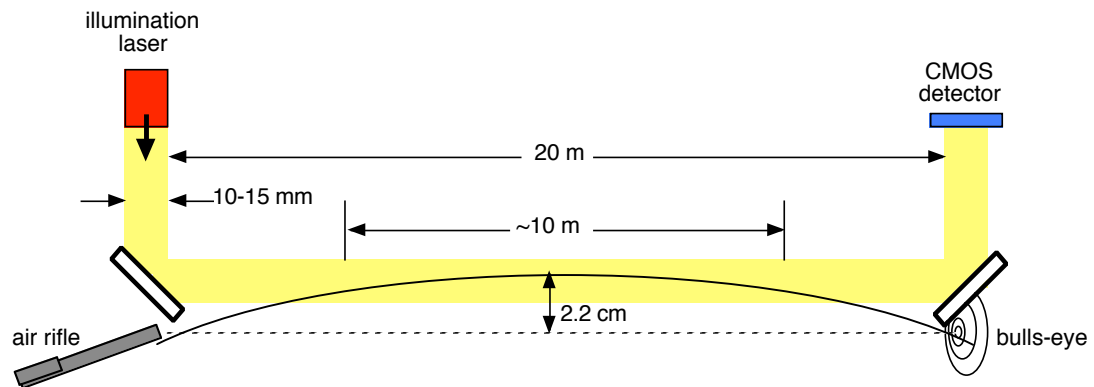

Figure 28 - Ballistic target trajectory through Poisson spot illumination beam

The pellet's velocity was observed to be traveling ~150 m/s at the end of its trajectory. This was the slowest the gun would fire a pellet without compromising accuracy, even the heaviest pellet we could find at 12 grains. We realized that this high of a velocity was unprototypic but we wanted to test the idea of the parabolic trajectory, which would eliminate the rotating mirror. By firing up into the beam, the pellet could be tracked for approximately half of the beam length. We also realized that the

centroiding algorithm was not able to adequately acquire enough data points to allow visualization of the pellet's motion. At best we were able to capture three frames "live."

Another simulation used a Photron FastCam camera that captured images at 1000 fps. We were not able to employ the centroiding algorithm calculations "live" because this camera stores the images to memory to be retrieved later. By using the FastCam, we were able to capture ~50 images of the Poisson spot in flight as it came up into the beam and then fell back down. The following (upside down) image sequence (figure 29) shows the Poisson spot's motion (very small and dark) in 10 ms intervals, although we captured every 1 ms.
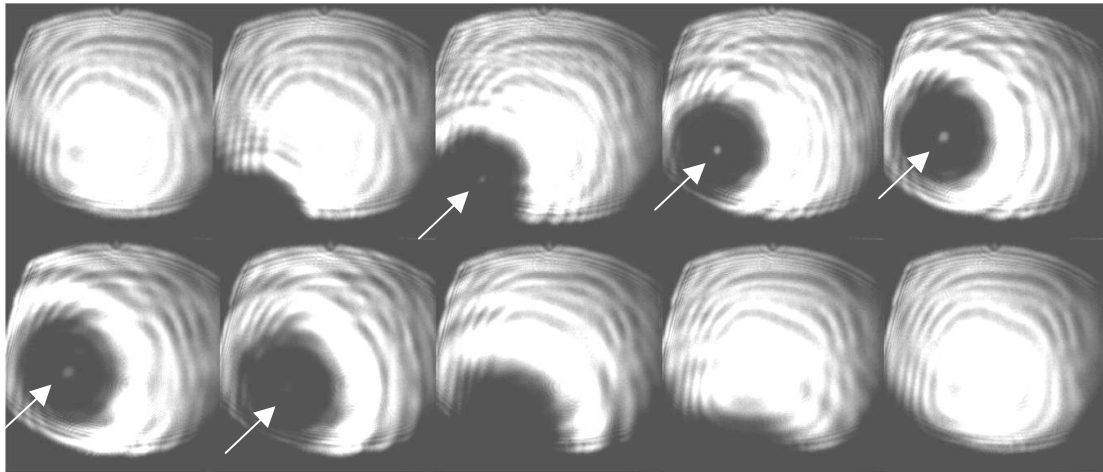

Figure 29 - 10 ms per frame video sequence of surrogate target coming into and out of the camera's FOV

The centroiding algorithm was then applied afterward to the saved images and the resulting x and y trajectories were plotted in the appendix in figures 38 and 39. We were also able to plot the Poisson spot's decreasing diameter as a function of target/detector's decreasing distance, as shown in figure 40. Additionally, we found that

gas ejecting from the muzzle disrupted the illumination beam and caused the image to waver slightly on the camera. Also, the air rifle has 12 rifling grooves with moderate twist, which help stabilize the pellet in midair. This spinning of the pellet also influenced the Poisson spot and caused it to waver and shimmer slightly.

VII.4 Next Generation Target Transport System

After working with the beam train for some time and observing its characteristic random motion, we began to realize that we needed to upgrade to a more prototypic method of moving the target. At the time of its implementation, the train appeared to be a stable way in which to move the target as well as verify correct beam steering on the PSD as well. However, the randomness of the plastic track on which it runs, while giving the FSM an erratic target to track, is not prototypic for an actual IFE power plant. In actuality, the target needs to be in free flight through a slight trajectory for a couple of meters to mimic an actual injected target, as well as have capability of being rep-rated. We felt that the most stable and non-fluctuating injection/transportation method would be gravity. Hence we have envisioned a vertical drop tower a meter or two above the optic table that will drop BBs through a slight arc into the PS illumination beam for tracking. Such a system will allow for integration of the zero-crossing and Doppler fringe-counting systems in the future. See figure 30 below for a conceptual sketch.
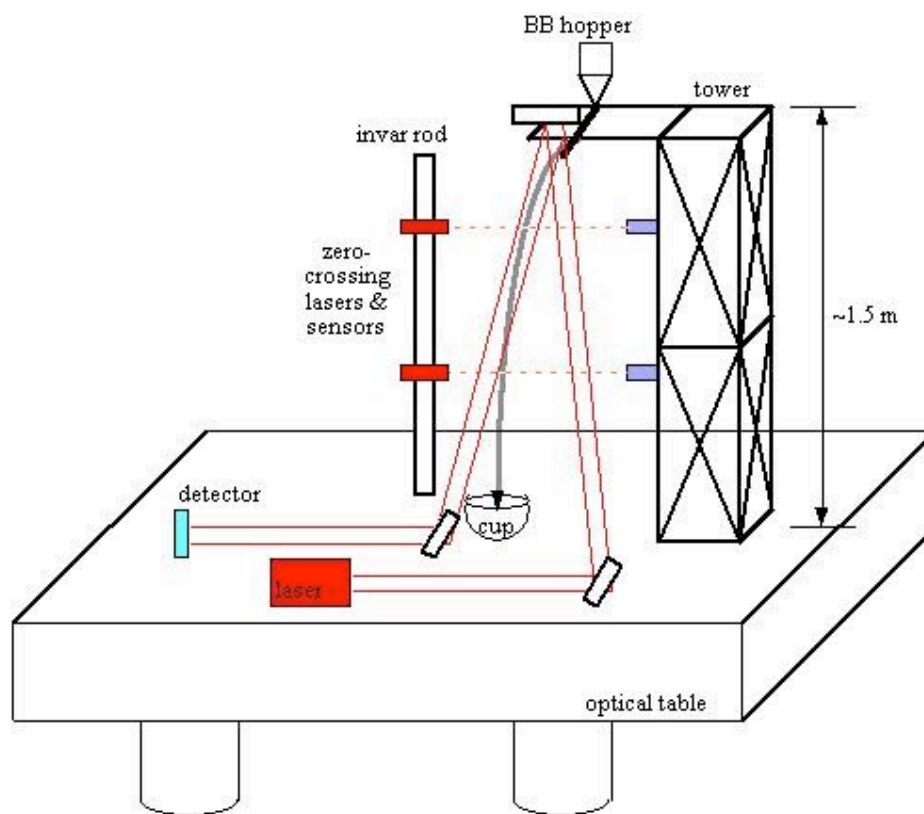
Figure 30 - Drop tower concept sketch

VIII. Integration of Subsystems (Tasks 7 & 9)

Integration so far has been shown above in the optical layout for the target engagement system in figures 5 and 6 at the beginning of chapter III. Throughout this project we have built upon several successful building blocks in the R&D plan. Two major integration accomplishments are the active feedback, continuous tracking from the Poisson spot and the on-axis beamlet steering demonstration. The first integration verified that we could indeed track the target "continuously" (every 20 ms). Although this task may seem trivial now, it incorporates and requires that the detection and centroiding of the Poisson spot, the simulated driver beam, the beam steering, and the target transport system all work together. A graph showing continuous tracking of the target is displayed below in figure 31. The x and y motion simply shows the target vibrating and rocking as the beam train transports it along the track.
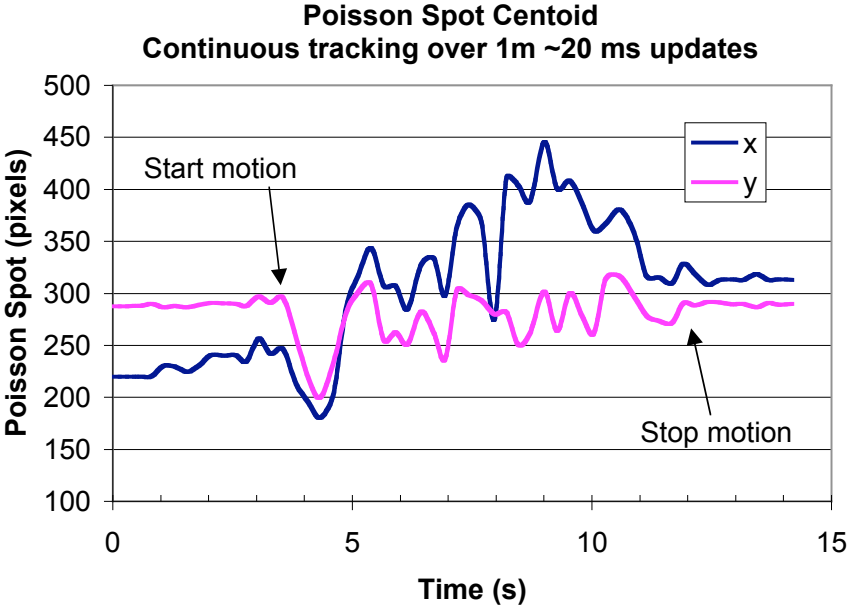

Figure 31 - Continuous tracking of the Poisson spot in both x & y directions

The second major integration involved demonstrating accurate, prototypic illuminating of the target by the driver beam as the target was transported down the track. This incorporated the open loop calibration of the driver beam and verification of correct illuminating of the target on the PSD. The results for this integration have already been shown above in figure 22 in the beam steering section. This graph shows the driver beam actively steering using the information from the centroiding algorithm to maintain illumination of the target even though it wandering about on the train track.

The integration of these components involved the combination of different ranges of motion as well as different coordinate system. The CMOS camera's chip has a detectable area of 6.4 x 4.8 mm. The PSD had a surface area of one square centimeter with a detectable, linear range of a little less than that (~8 x 8.5 mm). The FSM, as explained above, had to be modified with the telecentric lens configuration to reach the desirable range of motion for target illumination (~8 x 9.5 mm). These ranges are all fairly prototypic to the actual IFE power plant, but were sometimes difficult to stay within range due to the coordination needed between beams, sensors, and optics. The coordinate systems of the FSM, driver beam, camera, and Poisson spot illumination beam were all tied together on the floating optical table. The system that was moving, the PSD, was calibrated by the FSM location to steer on-axis as the target traveled down the track. For the off-axis demo to come, the coordinate system for the FSM will be different depending on its location and the range of motion will be limited to a 1 cm box.

The complete LabView timing breakdown for continuous, on-axis target engagement has already been discussed in detail in previous sections. The total

computational time for one update is ~23.5 ms with the current hardware and image processing algorithm. We initially used an NI Compact Vision System as a stand-alone unit for doing the processing. However, with only a 400 MHz chip, it fell far short of a conventional desktop PC's GHz processing power. The current hardware includes a Dell Dimension 3000 computer with a 3 GHz Pentium 4 processor and 1 GB of RAM running under Windows XP with LabView 7.1, National Instruments DAQ card, ThorLabs FSM, and Pacific Silicone Sensors PSD.

Table 4 below provides a preliminary timing sequence of the injection, tracking, and lasing of the target specifically relevant to the engagement system. These times and distances are approximated and generalized and serve mainly to present a sequential timeline of the events taking place in the tracking and steering system.

Preliminary Tracking Event Sequence Model for an IFE Power Plant
(Assume 5Hz repetition rate, 100 m/s injection velocity, and injection orientation is horizontal)

Approx. Time (ms):	Axial Position from Chamber Center (m):	Description of Event:
-200	-20	Target is injected toward chamber center
-185	-18.5	Target passes zero-crossing sensor; Poisson spot and axial tracking begin
-175	-17.5	Target is tracked along its trajectory toward chamber center, preliminary implosion position calculated
-165	-16.5	FSMs begin to correct for large offsets from previous shot
-100	-10	Target is halfway to chamber center at apogee
-50	-5	Predicted target location is updated every few ms and becomes more refined
-25	-2.5	FSMs continue to correct driver beam pointing for smaller offsets
-1.5	-0.15	Glint laser fires
-1	-0.10	All beamlet FSMs commence fine tuning to final position
-0.003	-0.0003	Driver beams fire
0	0	Engagement
+0.003	+0.0003	FSMs "zoom" and follow imploding target
		All FSMs hold position until next target's update

Table 4 - Preliminary tracking event sequence model for an IFE power plant

IX. Achievements, Conclusions, & Recommendations

We have successfully accomplished and exceeded the goal of this thesis to build, characterize, and demonstrate an active target tracking and beam steering system for laser IFE. We have completed the portion of the R&D plan that we proposed at the conceptualization of the project and have met preliminary time, speed, and accuracy requirements. Recommendations for the next generation target engagement system have been given for each corresponding subsystem. Forthcoming work on the engagement project to integrate the entire R&D plan is spelled out very clearly and will continue for the next few years.

Appendix

Resources

Thor Labs http://www.thorlabs.com Optical components, FSM

Edmund Optics http://www.edmundoptics.com Optical components

Physik Instrumente (PI) http://www.pi.ws FSM

Piezosystem Jena http://www.piezojena.com Piezo actuators, FSM

National Instruments (NI) http://www.ni.com Compact vision system, LabView, DAQ

Basler Vision Technologies http://www.baslerweb.com CMOS camera

Dell Computers http://www.dell.com PC computer

NI LabView Algorithm Screenshots
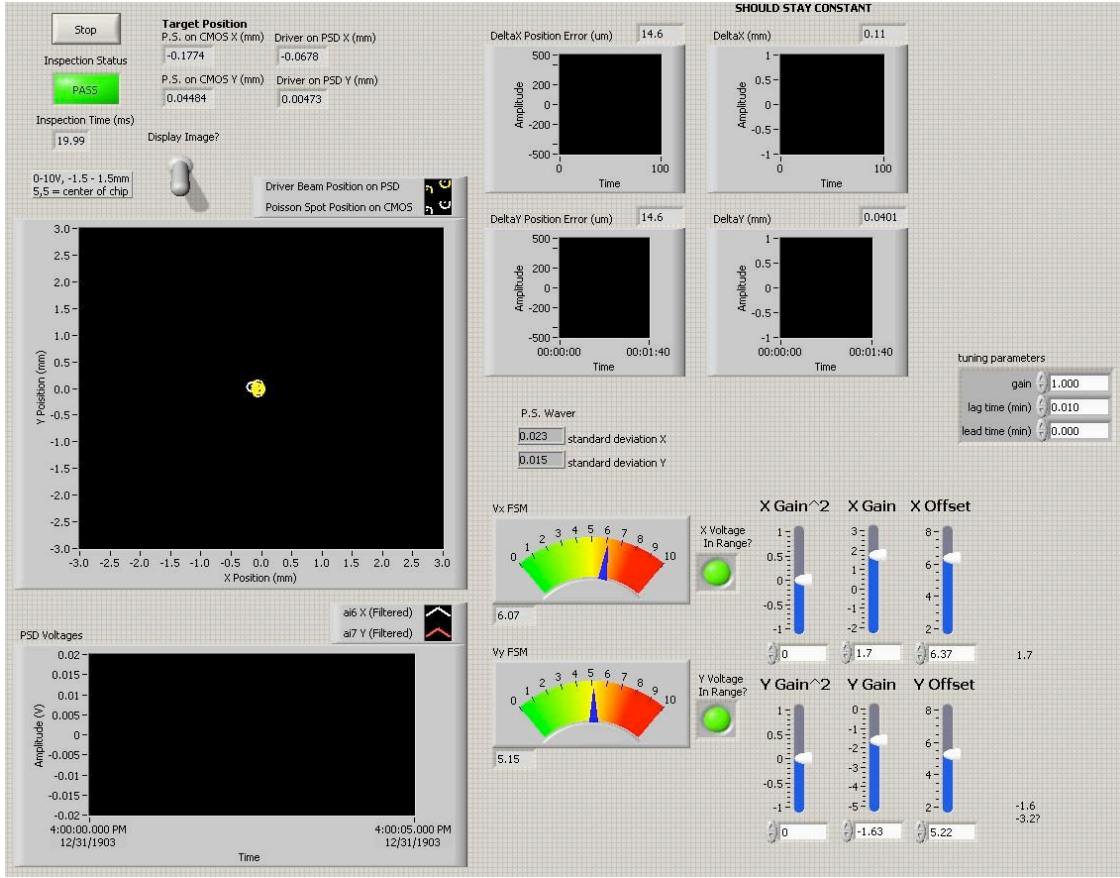
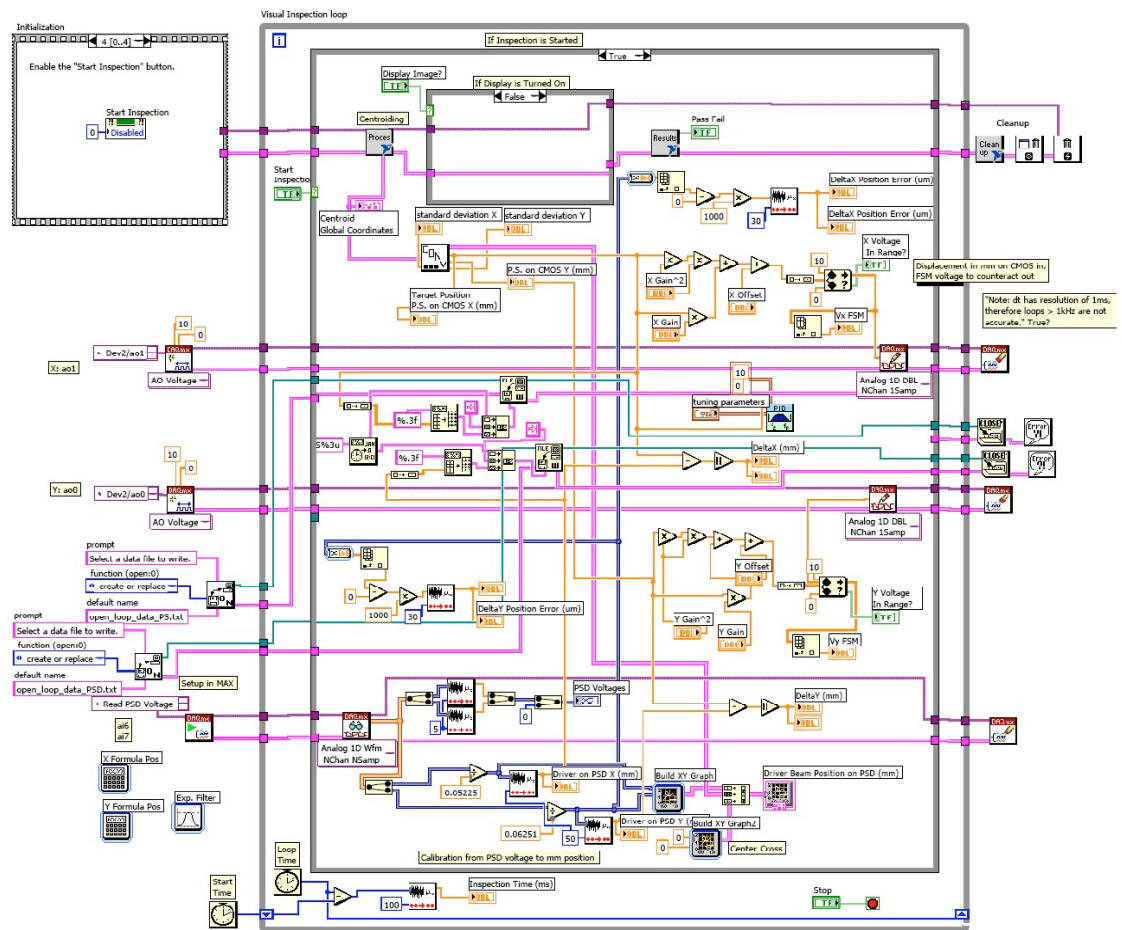Figure 32 - LabView's target engagement front panel

Figure 33 - LabView's target engagement back panel connections

Additional Pictures & Graphs

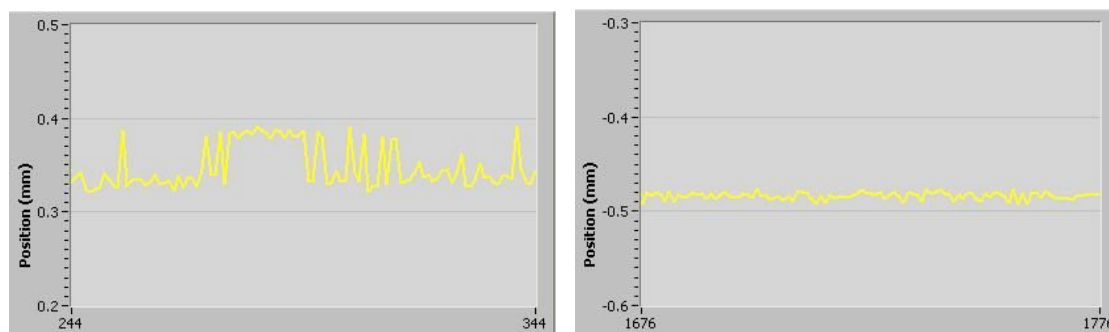Figure 34 - Plastic tent sheeting used to minimize air currents

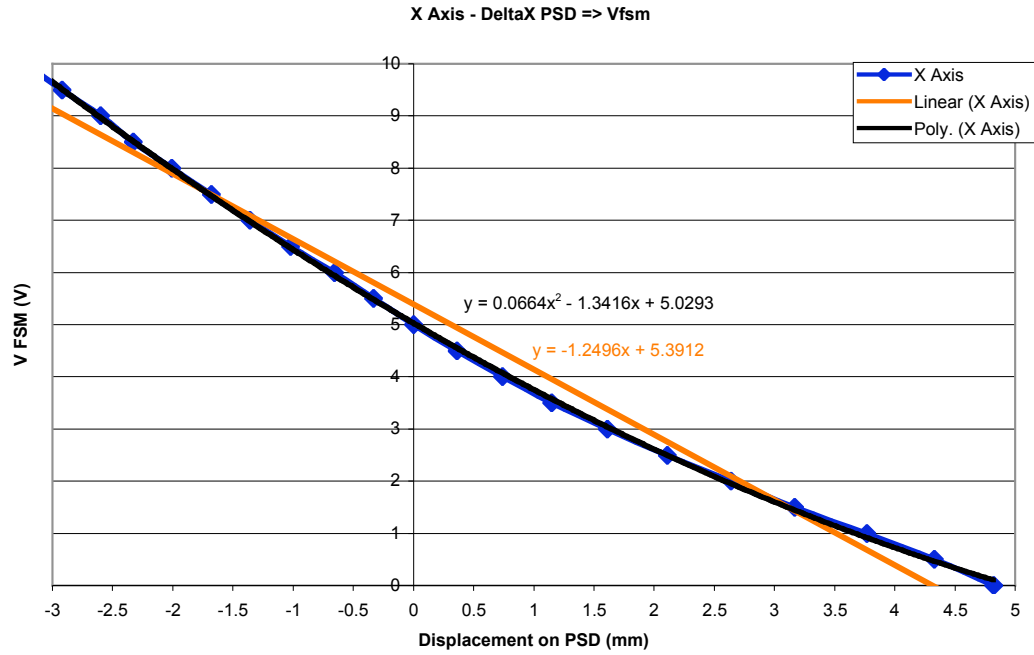Figure 35 - Beam wavering reduction on PSD without plastic tent (L) and with tent (R)

X Axis - DeltaX PSD => Vfsm

$$y = 0.0664x^2 - 1.3416x + 5.0293$$

$$y = -1.2496x + 5.3912$$

Figure 36 - X-axis PSD displacement to FSM voltage calibration with linear and polynomial fits

Y Axis - DeltaY => Vfsm

$$y = 0.0475x^2 - 1.1585x + 4.9206$$

$$y = -1.0931x + 5.2657$$
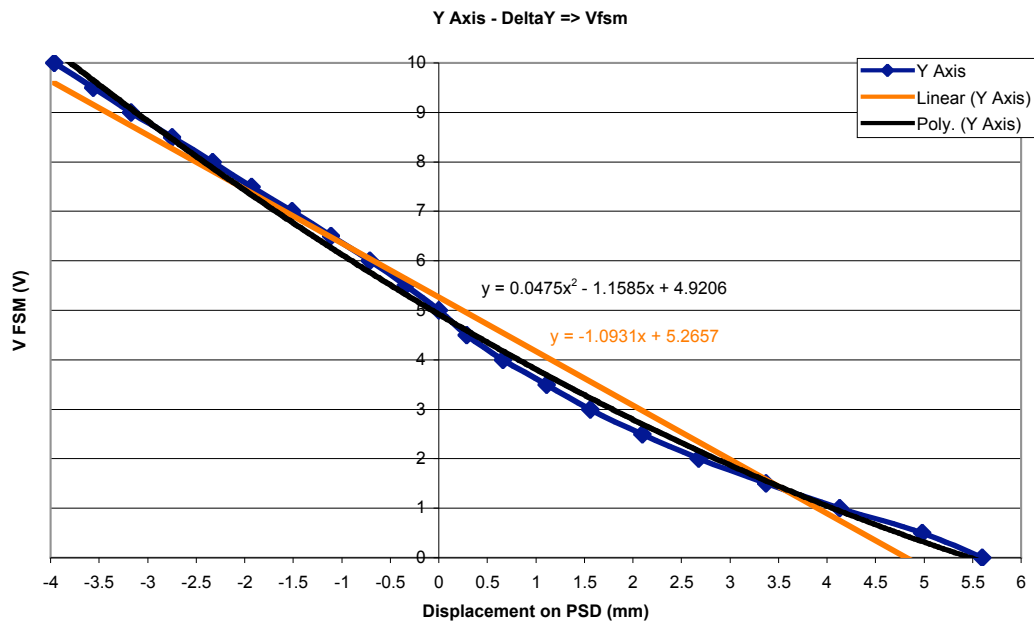
Figure 37 - Y-axis PSD displacement to FSM voltage calibration with linear and polynomial fits

Shot 054 X-Axis Centroid Location

$y = -0.0038x^3 + 0.8711x^2 - 64.695x + 2300.8$
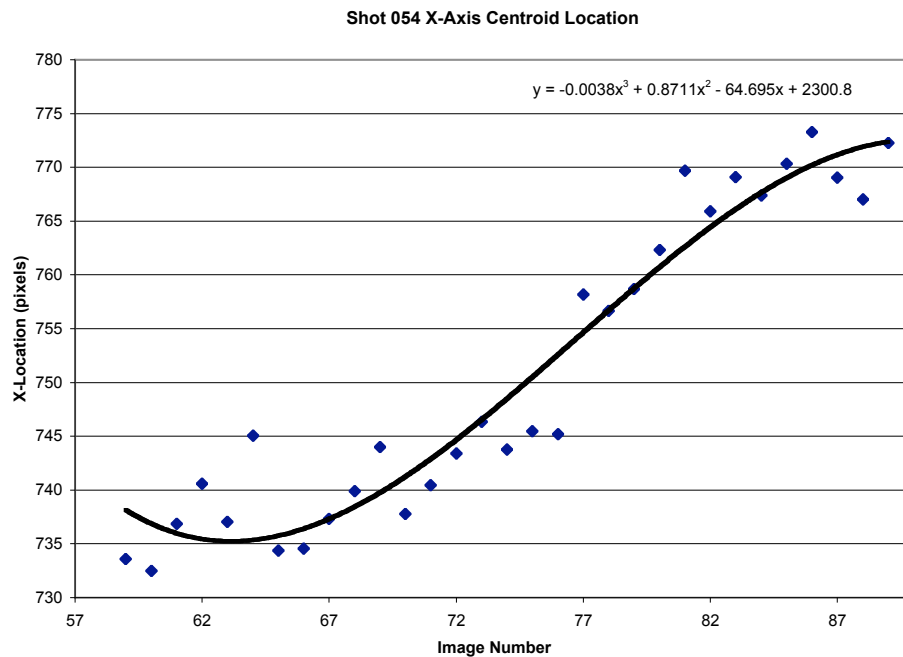
Figure 38 - X-axis (horizontal) air rifle target tracking showing wavering of pellet in mid-flight

Shot 054 Y-Axis Centroid Location
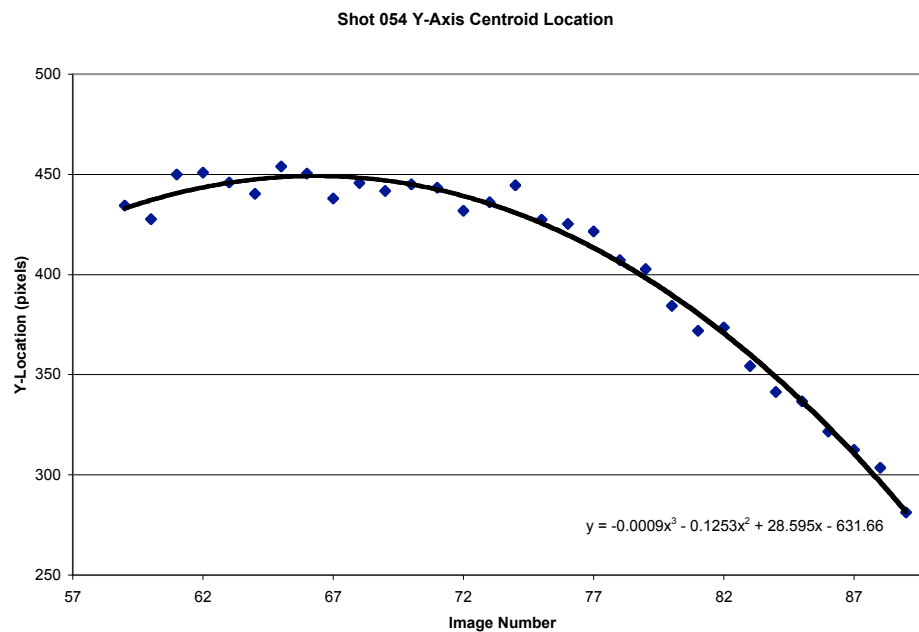

$y = -0.0009x^3 - 0.1253x^2 + 28.595x - 631.66$

Figure 39 - Y-axis (vertical) air rifle target tracking showing parabolic trajectory of the pellet in mid-flight

Shot 054 - Poisson Spot Diameter
(Simulated Algorithm)

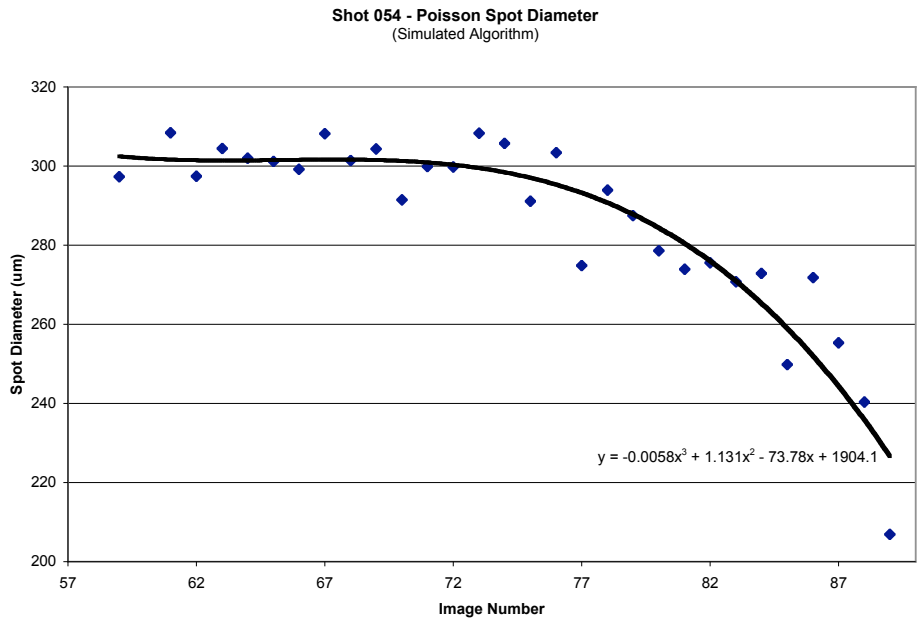$$y = -0.0058x^3 + 1.131x^2 - 73.78x + 1904.1$$

Figure 40 - Poisson spot dynamic diameter from air rifle target tracking decreases as target/detector distance decreases
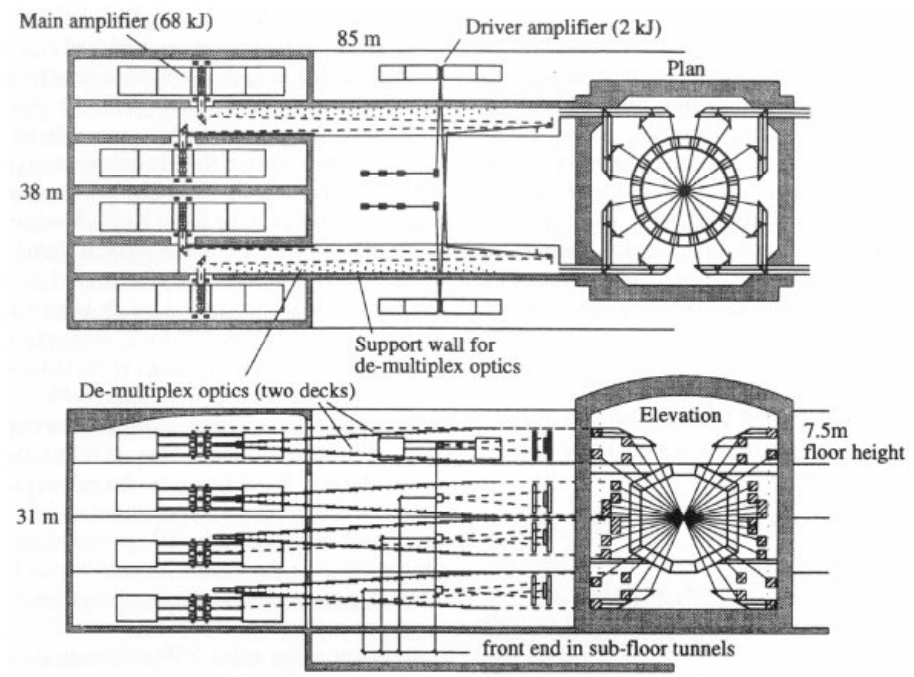

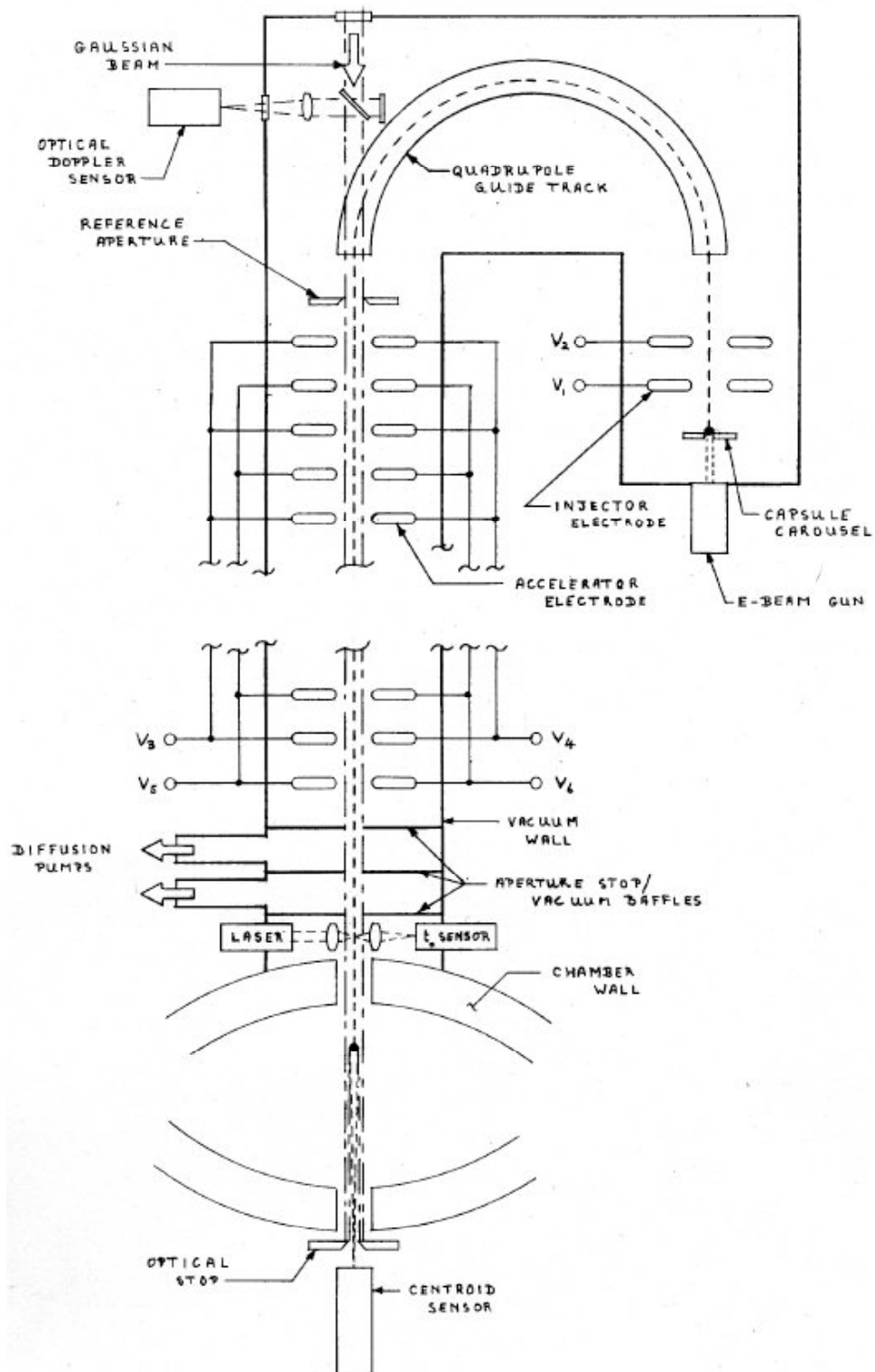Figure 41 - Plan and elevation of a 2-MJ KrF laser facility [17]

Figure 42 - Electromagnetic injection and steering concept frees the axial beam path [7]

References

[1]   R.L. Murray, "Nuclear Energy," Butterworth-Heinemann, Fifth Edition, Woburn, MA, 2001.

[2]   M.S. Tillack, "IFE Technology Research at UC San Diego," MAE Department Presentation, October 6, 2004.

[3]   G. Flint, "Integration of IFE Beamlet Alignment, Target Tracking, and Beam Steering," HAPL Presentation, NRL, Washington, D.C. March 3, 2005.

[4]   J. D. Sethian, M. Friedman, R. H. Lehmberg, M. Myers, S. P. Obenschain, J. Giuliani, P. Kepple, A. J. Schmitt, D. Colombant, J. Gardner, F. Hegeler, M. Wolford, S. B. Swanekamp, D. Weidenheimer, D. Welch, D. Rose, S. Payne, C. Bibeau, A. Bayramian, R. Beach, K. Schaffers, B. Freitas, K. Skulina, W. Meier, J. Latkowski, L. J. Perkins, D. Goodin, R. Petzoldt, E. Stephens, F. Najmabadi, M. Tillack, R. Raffray, Z. Dragojlovic, D. Haynes, R. Peterson, G. Kulcinski, J. Hoffer, D. Geller, D. Schroen, J. Streit, C. Olson, T. Tanaka, T. Renk, G. Rochau, L. Snead, N. Ghoniem and G. Lucas, "Fusion Energy with Lasers, Direct Drive Targets, and Dry Wall Chambers," *Nuclear Fusion* **43** (2003) 1693-1709.

[5]   R. Petzoldt, D. Goodin, E. Valmianski, N. Alexander, J. Hoffer, "Update on Various Target Issues," HAPL Presentation, June 21, 2005.

[6]   M.S. Tillack, D.T. Goodin, N.B. Alexander, R.W. Petzoldt, A.R. Raffray, D. Schroen, J.D. Sethian, J.E. Streit, "A Target Fabrication and Injection Facility for Laser-IFE," 20th IEEE/NPSS Symposium on Fusion Engineering (SOFE), San Diego, CA, October 14-17, 2003.

[7]   G. Flint, "Acceleration and Tracking of Direct-Drive Fusion Targets," Unpublished paper, September 2, 2004.

[8]   A. E. Siegman, "Lasers," University Science Books, Sausalito, CA, 1986.

[9]   W.B. Herrmannsfeldt, "SLAC alignment System," SLAC-PUB-222, Stanford Linear Accelerator Center, Stanford University, Stanford, CA, October 1966.

[10] L.V. Griffith, R.F. Schenz, G.E. Sommargren, "Magnetic alignment and the Poission alignment reference system," *Rev. Sci. Instrum.* **61**, August 1990.

[11] J.A. Harvey, J.L. Forgham, "The spot of Arago: New relevance for an old phenomenon," *Am. J. Physics.* **52**, March 1984.

[12] National Instruments, "IMAQ Vision Concepts Manual," 11.1 – 11.13, 12.1 – 12.10, Austin, TX, June 2003 ed.

[13] M.K. Cheezum, W.F. Walker, W.H. Goilford, "Quantitative Comparison of Algorithms for Tracking Single Fluorescent Particles," *Biophysical Journal* **81**, October 2001.

[14] J. D. Sethian, "Electron Beam Pumped Krypton-Fluoride (KrF) Lasers for Fusion Energy," Presentation, APS DPP 2002.

[15] M. McGeoch, "Elements of IFE Design," Unpublished paper, May 12, 2005.

[16] T. Lehecka, R.H. Lehmberg, A.V. Deniz, K.A. Gerber, S.P. Obenschain, C.J. Pawley, M.S. Pronko, C.A. Sullivan, "Production of High Energy Uniform Focal Profiles with the Nike Laser," *Optics Communications* **117**, (1995) 485-491.

[17] M.W. McGeoch, P.A. Corcoran, S.E. Bodner, R.H. Lehmberg, S.P. Obernschain, J.D. Sethian, "Conceptual Design of a 2-MJ KrF Laser Fusion Facility," *Fusion Technology* **32**, (1997) 610-643.

[18] T. Lehecka, "KrF Laser Optical Train and Staging," HAPL Presentation, June 21, 2005.